Answer

Interactive comment on "High-resolution diapycnal mixing map of the Alboran Sea thermocline from seismic reflection images" by Jhon F. Mojica et al.

Anonymous Referee #1

Received and published: 10 October 2017

General Comments:

The paper presents some nice data acoustic data from the Alboran Sea, for which turbulent mixing estimates within the thermocline have been estimated at high spatial resolutions. mixing estimates show an interesting 'patchyness'. Some oceanographic data has also been used to compare mixing rate estimates. Overall the paper is well put together and the data well presented. However, I feel that the paper requires some further work on three counts:

We thank reviewer#1 for the constructive comments and review that has surely helped to improve the manuscript. We have taken all comments and suggestions into account as indicated in our point-by-point answers below.

1 - Clarification should be provided regards the physical mechanisms behind the mixing distribution observed. Messages regards the influence of internal waves seem confused.

We agree that the relationship between observed oceanographic features and mixing distribution was unclear. Our main message is that there is not a clear correspondence between the location of IWs (> 100 m horizontal scale) and mixing hotspots, but rather between mixing hotspots and the location of large-amplitude features in the transitional domain (30-100 m horizontal scale). Based on this analysis as well as on previous results presented in Sallares et al (2016), we interpret that these large-amplitude features are the expression of shear instabilities (e.g. KH-type billows). This means that there is not a direct relationship between IWs and mixing. It tends to concentrate where IWs become unstable and instabilities develop, leading to turbulence. We clarify this message in the new version of the text (line 19-21, line 339-341, line 383-386).

2 - The analysis of mixing-rates from oceanographic data, using fine-structure estimates (and assumptions therein) needs to be improved - see comments below

See answer below (comments line 165).

3 - I would like to see a comparison of mixing estimates form the internal wave and Batchelor regimes of the MCS spectra

We have estimated the $k_\rho(x,z)$ map for internal waves and Batchelor regimes (figure rev.1-1). The lower mixing values produced by IWs as compared to the Batchelor regime are clear.

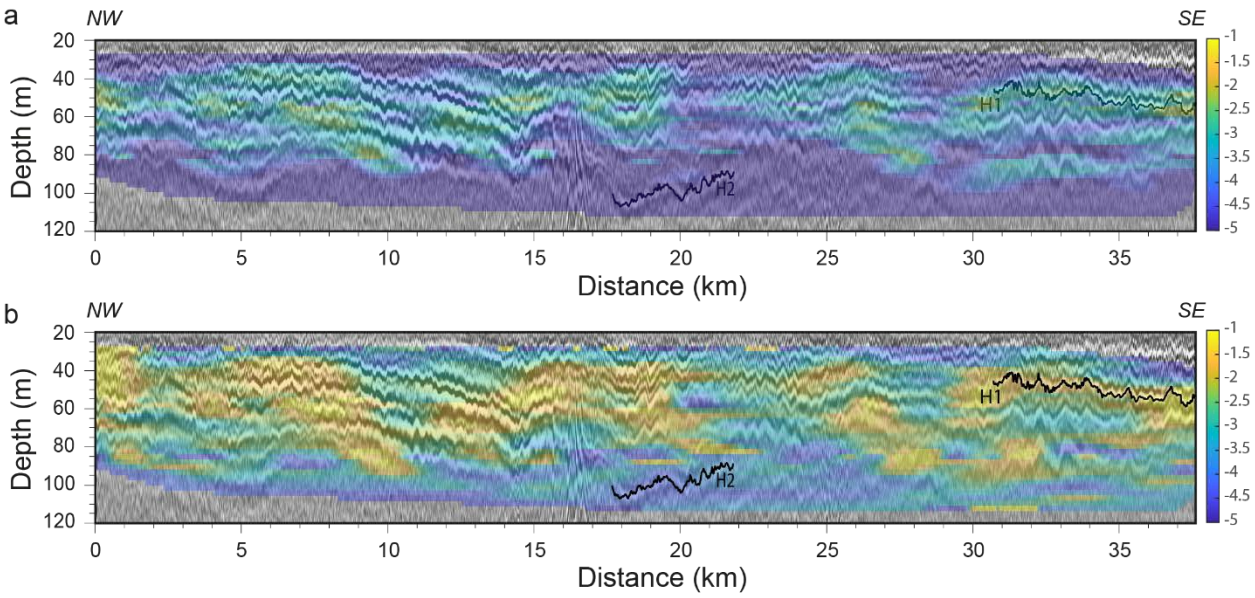

Figure rev.1-1. High-resolution $k_\rho(x, z)$ map overlapped with the HR-MCS image. Solid lines labelled H1 and H2, display acoustic reflectors located within relatively high- and low-dissipation areas (a) from internal waves Gregg89 model (b) and from Batchelor59 model.

Specific comments:

Lines 35-37: Please clarify here - I think that both your references refer to internal-wave phenomena

Thanks for the comment, references have been corrected (line 38).

Lines 50-53: I am not sure what you are saying here.

We just want to describe the behavior of ε in a conservative flow. We have modified the text to make this point clear (line 51-52).

Lines 65: I think that lowered microstructure profiles are generally the most robust source of turbulent measurements.

We agree, of course. Our point here was to note that these devices (VMP, microriders), provide measurements in just one dimension (either horizontal or vertical), but seismic data cover both dimensions at once. It is obviously with poorer resolution than microstructure profilers, but much better than that of conventional probe-based studies in the horizontal one (line 63-65)

Line 150: Do you have evidence for this? Could you compare acoustic reflection horizons to density horizons in the oceanographic data?

We do not have direct evidence for this particular profile because we cannot invert density with this data and we do not have the appropriate complementary oceanographic data.

However, in a previous study by our group with appropriate data, we showed that seismic reflectors do actually follow isopycnals (Biescas et al, 2014).

Line 165: If possible you should use integrated shear and or strain spectra to get estimates from CTD/ADCP data - perhaps you are limited by depth ranges? You are also missing some terms in for shear-to-strain ratio and inertial frequency e.g. see Waterman, S., K. L. Polzin, and A. C. Naveira-Garabato (2012), Internal waves and turbulence in the Antarctic Circumpolar Current, J. Phys. Oceanogr., 43, 259–282. You should at least quantify the omission of these terms and also explain how you decide on what you mean by 'uncertainty bounds' in several places in the text. You should also mention the errors associated with fine-structure estimates - particularly in regions away from the open ocean.

Assuming the energy dissipation in the thermocline (depth range <120m), we follow the Gregg89 model, where the observations agree with the predictions sufficiently well to suggest that the simplest way to obtain average dissipation rates over large space and time scales is through $N^2/N_0^2 < S_{10}^4/S_{GM}^4 >$ (Gregg, 1989). This model is commonly applied in the mid-latitude thermocline as our observations. That is why we use this simple but accurate model. On the other hand, Waterman et al. (2013) consider the relation:

$$R_\omega = \langle V_Z^2 \rangle \Big/ (\bar{N}^2 \langle \zeta_Z^2 \rangle) \quad (1)$$

The main term omitted for us is (ζ_z) the relative local change in buoyancy frequency from background:

$$\zeta_z = (N^2 - N_{ref}^2)/N_{ref}^2 \quad (2)$$

For our data this value is ~0.9. This value can be related with the level of stretching and squeezing of isopycnals by internal waves, but as it is close to 1, the incidence is not relevant in our case (line 162-165).

Saying that the results agree "within uncertainty bounds" was an overstatement, so we have changed this in the new version. What we actually meant is that the global average and the values obtained with the XCTD are "within the range of values" obtained from the seismic data analysis. We have reworded the text accordingly (line 22-24, 245-246, 376-379).

Lines 195-200: This should be in methods

Done (line 191-199)

Line 203: Spatial resolution - be careful what you mean by this as really each data point is an average over 1200m by 15 m box

Yes, we agree. We must distinguish between the theoretical resolution of the seismic data and that of the diapycnal mixing maps. For seismic data, the vertical resolution (i.e. the capability to discern between neighboring reflectors) is given by the Rayleigh criteria, whereas the horizontal resolution (i.e. the part of a reflector covered within half a wavelength of the seismic signal) corresponds to the first Fresnel zone. For our acquisition system, medium properties, and target depth, these are ~2 m and ~15 m respectively (it is explained in Sallares et al., 2016). However, this does not represent the resolution of the mixing map. In this case, we are calculating spectra and diapycnal mixing within windows of 1200x15 m, so this could be taken as the approximate resolution of the map. We have modified the text accordingly (line 197-199).

Lines 215: What scale are you computing shear over i.e. dZ? Also how to you quantify buoyancy frequencies, N?

(Line 221) dz is 10 m. To calculate buoyancy frequency we use the expression below, where density is obtained from the XCTD data:

$$N = \sqrt{-\frac{g}{\rho_0}\frac{\delta_\rho(z)}{\delta_z}} \qquad (3)$$

Lines 319: Shear to strain ratios tell you about the frequency content of the internal wave field. You might well expect higher inertial content (i.e high shear to strain ratios) near the surface due to wind generation.

As we describe below the level of stretching and squeezing of isopycnals by internal waves, is close to 1. Near the surface we would expect higher inertial content, but we consider the whole thermocline, where we can see a trending a robust regularity over the whole profile (figure rev1-1). This variation is consistent with the process already described in Sallares et al. (2016).

Lines 325: How do dissipation estimates compare for GM and Batchelor parts of the MCS spectra? This may tell you something about the role of IW in generating the turbulence/GM assumptions

As it is shown in figure rev.1-1 and it is explained above, the general patterns in the diffusivity maps obtained with the GM (a) and Batchelor (b) parts of the spectra (including location of maximum and minimum values) are very similar. It appears to be a clear correspondence between the two diffusivity maps. However, the values obtained from the Batchelor part of the spectra are much higher than those obtained from the GM part. To us, this indicates the stronger influence of instabilities, rather than IWs, on diffusivity.

Line 334 and 351: Confusing regards what you are trying to report regards role of internal waves here - please clarify.

As we explained above, our main point is that we do not see a direct relationship between IWs and mixing. Mixing appear to concentrate where IWs become unstable and

instabilities develop, leading to turbulence. We have tried to clarify this message in the new version of the text (line 248-250, 334-336, 383-386).

Answer

Interactive comment on "High-resolution diapycnal mixing map of the Alboran Sea thermocline from seismic reflection images" by Jhon F. Mojica et al.

Anonymous Referee #2

Received and published: 11 October 2017

This manuscript presents seismic reflection data from the Alboran Sea and outlines a method for producing a map of diapycnal diffusivity across one profile. The major conclusion is that the profile shows patchy turbulence on the scale of a few kilometers horizontally and 10-15 meters vertically. Further, the authors observe greater mixing in areas of internal wave instability. Results are compared to estimates of turbulence made from XCTD and ADCP data as well as background reference models. Additional analyses of filtered slope spectra examine the relationship between diapycnal mixing and the assigned internal wave and transitional subranges.

First, we want to thank referee#2 for her/his effort. We found the comments and suggestions very useful, and we have tried to answer and/or follow all of them as indicated in our point-by-point answers below.

The introduction and background are clearly written and well presented. However, the manuscript takes on the substantial challenge of developing a new method and presenting scientific conclusions at once, and in a relatively short format. As a result, I think many issues addressing the methods, presented data, clarity of conclusions, uncertainties, and reach of results are insufficient.

Thanks for the comment. We first want to make clear that the goal of the paper is not presenting the details of the data processing and spectral analysis, nor developing a new method to estimate mixing. The method used to produce the diapycnal diffusivity map from seismic data is not new; it is analogous to that presented in previous works (i.e. Sheen et al, 2009; Holbrook et al, 2013). In addition, the seismic data and their spectra were recently processed, analyzed and interpreted in detail in another paper by our group (Sallares et al. 2016). In fact, many of the questions raised by referee#2 are addressed in this paper. We have modified the text to make it clearer in the new version of the manuscript (line 100-102, 137-141).

We would like to emphasize that our goal and original contribution of the paper are (1) producing a diapycnal mixing map of higher resolution than any previously existing one and (2) applying it for the first time to shallow waters (thermocline), a critical area to study mixing processes. We then try to interpret the observed features based on the results but also on our previous work. To do this, we use data acquired in the Alboran basin with high-resolution multichannel seismic system, which were presented, processed, analyzed and interpreted by Sallares et al. (2016). The basic points of the method applied to produce the maps are explained in this manuscript, and the details can be found in the

other two works mentioned above. We clarify this in the new version of the manuscript (lines 186-189 rewritten).

Major Concerns: Data handling and methods are insufficiently explained. The authors need to be clearer about the stated resolution. It is not accurate to apply a 1200x15 m grid to a 30x3 m grid and claim improved resolution. Many of the 30x3 m cells will not have tracks in them. In fact, at CMP spacing of 7.5 m, you can only have 4 or 5 traces represented (depending how you treat them) and few realistic and meaningful spectra can be taken at that scale.

The size of the window to calculate the spectra and to estimate the mixing values is always 1200 m wide x 15 m high. The difference with previous similar works is that the windows overlap with each other; The center of the window moves only 30 m in horizontal, and 3 m in vertical in each step. By doing this, the transition is smooth because we incorporate few new data in each new analyzed window. We can see the effect in figure rev2-1. (a) Mixing map obtained following a "conventional" way (i.e. no overlapping windows). In this case we apply a step of dx=1200 m, dz=6 m between 1200 m wide x 6 m high neighboring windows. (b) Mixing map obtained using 1200 m wide x 15 m high overlapping windows and a dx=30 m, dz=3 m step. The distribution and $k_\rho(x,z)$ values is equivalent to (a) but display smoother transitions, making the map look more "realistic". This type of representation is new, but as we stated above, the method to estimate $k_\rho(x,z)$ based on the horizontal wavenumber spectra of seismic reflectors is not new. We clarify all this in the new version of the manuscript (lines 197-199, 272-273, 298-300).

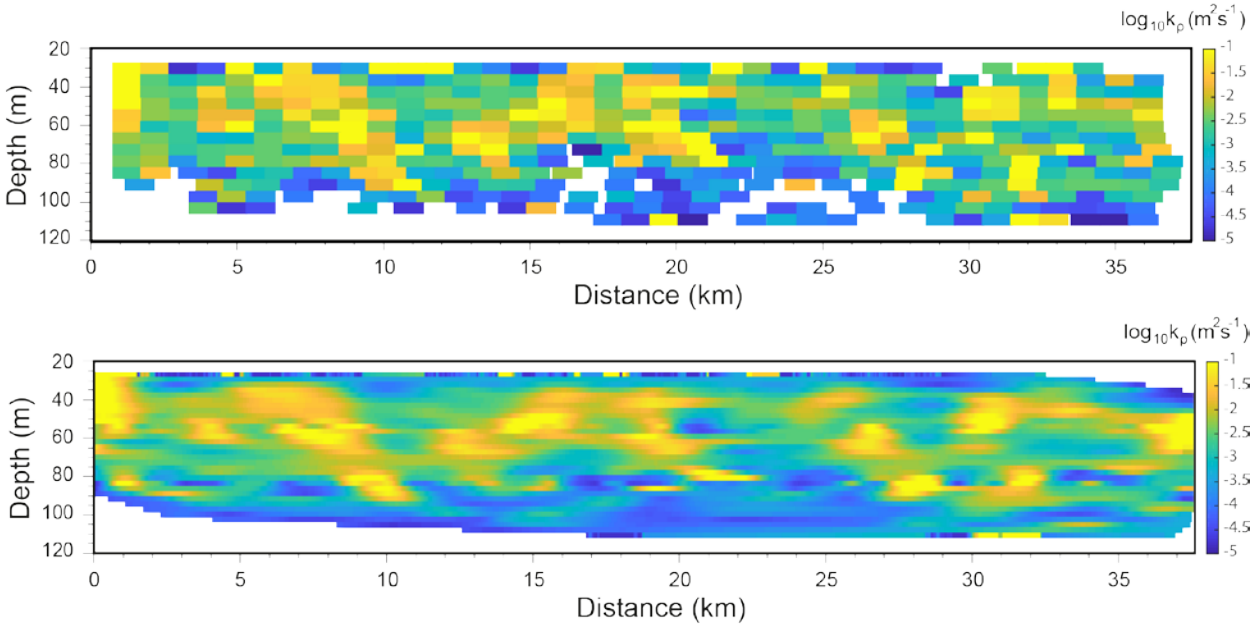

Figure rev2-1. $k_\rho(x, z)$ map obtained along the seismic profile. (a) without sliding window, using window size (1200 x 6 m) just getting one point for each window move, (b) applying sliding

window, using window size (1200 x 15m) with step (dx=30, dz=3m). The trends and values are equivalent, but (b) looks more continuous and, to us, more realistic.

The authors need to explain what happens when tracks are longer than the 1200 m box.

We cut the long tracks in 1200 m-long segments so that they fit inside the windows. This does not affect the spectrum at the spatial range analyzed. As an example, we analyze in figure rev2-2 a 16 km-long reflector (H3). We first calculate the spectrum for the whole reflector and we then split it in 10 segments (1.6 km each), and calculate their individual spectra as well as the average. The average spectra is very similar to the complete one in terms of energy and slope at the scale of interest. The details on the procedure followed to calculate the spectra can be found in Sallares et al. (2016) (line 193-194).

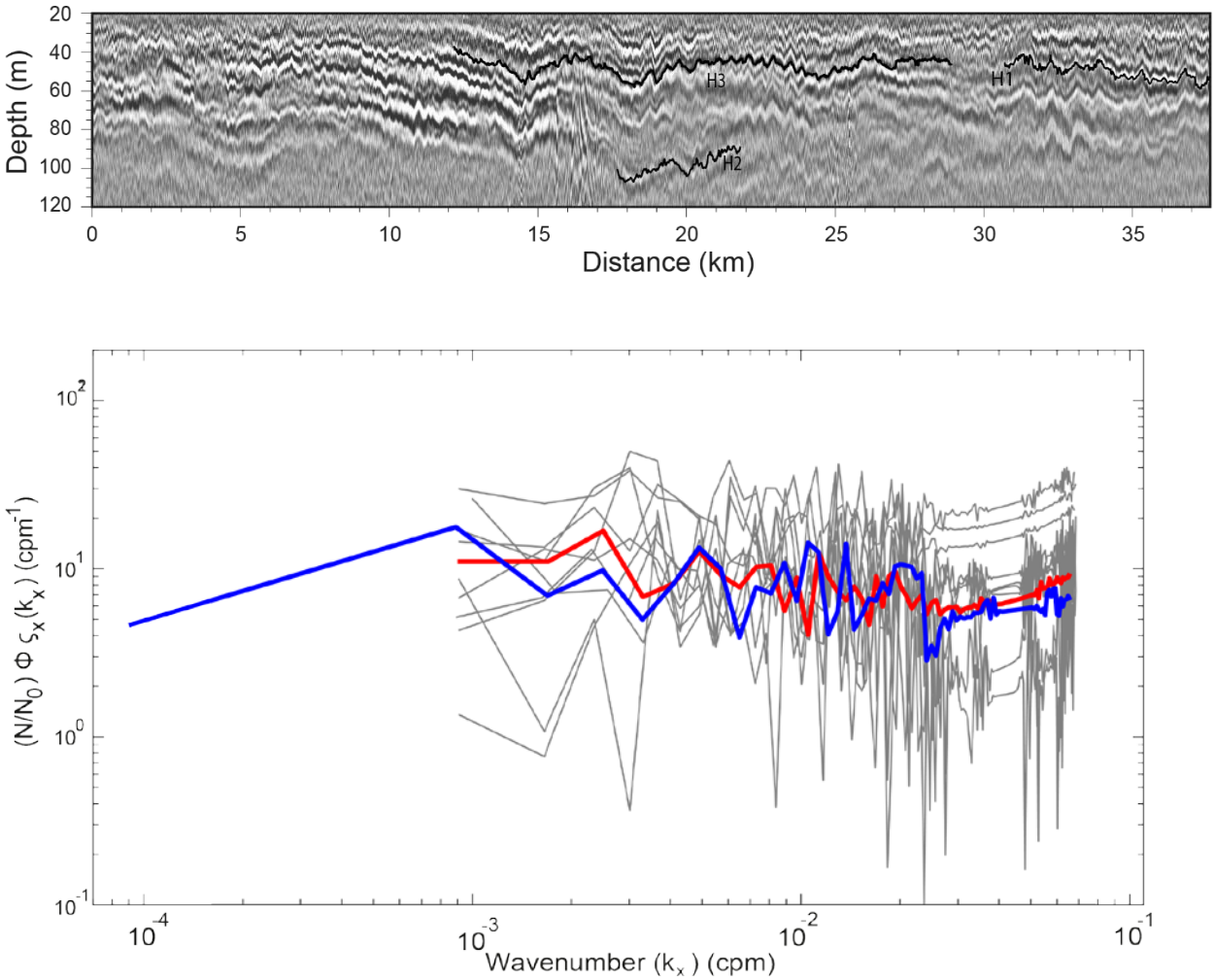

Figure rev2-2 (a) Depth-converted high-resolution multichannel seismic profile (Here we show a new horizon H3). (b) Horizontal spectrum of the vertical displacement of reflector H3. (blue line) considering the whole reflector. (gray lines) spectrum from the reflector split in ten 1.6 km-long

segments. (red line) average spectrum from the 10 segments. The average of the 10 segments and the whole reflector show the same trends in the scales of interest.

They state the tracks are 1.5-21 km long, so no tracks would fit inside the 1200 m grid length and position vertically is also unaddressed. Each track would be included in hundreds of 30x3 m grid cells which seriously undermine any claims at resolving patchy turbulence at their stated resolution.

As we already explained above: (1) 30x3m is not the grid cell, it is just the step applied to analyze a new “1200 m-long x 15 m-high” window. (2) The size of the windows (so that of the actual grid cells) is always 1200x15m. (3) The tracks longer than 1200 m are cut into smaller segments that fit inside the window.

Concerning resolution, we must distinguish between the theoretical resolution of the seismic data and that of the diapycnal mixing maps. For seismic data, the vertical resolution (i.e. the capability to discern between neighboring reflectors) is given by the Rayleigh criteria, whereas the horizontal resolution (i.e. the part of a reflector covered within half a wavelength of the seismic signal) corresponds to the first Fresnel zone. As we explain in Sallares et al. (2016), for our acquisition system, medium properties, and target depth, these are 1-2 m and 12-15 m, respectively. However, this does not represent the resolution of the mixing map. In this case, we are calculating spectra and diapycnal mixing within windows of 1200x15 m, so this could be taken as the approximate resolution of the map (in fact resolution is higher thanks to the “sliding window” approach). In summary, we do not claim that we are resolving structures of 30x3m, but the clear, larger-scale yellowish patches of 1-3 km-wide x 10-20 m-thick that are clearly identified in the map (better explained now in lines 209-212).

The authors need to show more of the data that support their methods and conclusions, particularly the reflector tracks and many more spectra.

As we explained above, our study builds on previous work concerning both method and data. The method to produce diapycnal mixing maps based on horizontal wavenumber spectra of seismic reflectors is described in Sheen et al. (2009) and Holbrook et al. (2013). The data, including acquisition system, MCS data processing, reflector tracking, S/N estimation, spectral analysis and statistical analysis of the obtained spectra, are presented in detail in Sallares et al. (2016) (in the main documents and supplementary material). We do not think that it is necessary to repeat what is already explained and shown in these papers, but we could add part of it as supplementary material if the referee and editor think otherwise (e.g. figs. Rev2-3 or 2-4). In any case, we have introduced several changes in the text to clarify this (line 100-101, 186-189).

To establish this as both a methods paper and support their science conclusion, these data must be shown and clear. First, show the 68 reflector tracks and discuss their distribution, including why application of a k value obtained on the large scale can be applied to the small scale and how to handle regions lacking tracked reflectors.

As we explained above, the original data, including the 68 reflectors and the criteria to select and track them, are shown and described in Sallares et al (2016). As you can see in figure rev2-3, they are rather homogeneously distributed throughout the analyzed area (30-110 m depth), so most of the 1200x15m analyzing windows contain reflectors and contribute to create the map. The few that do not have enough data to calculate the spectra are shown in white. We clarify this in lines 137-141.

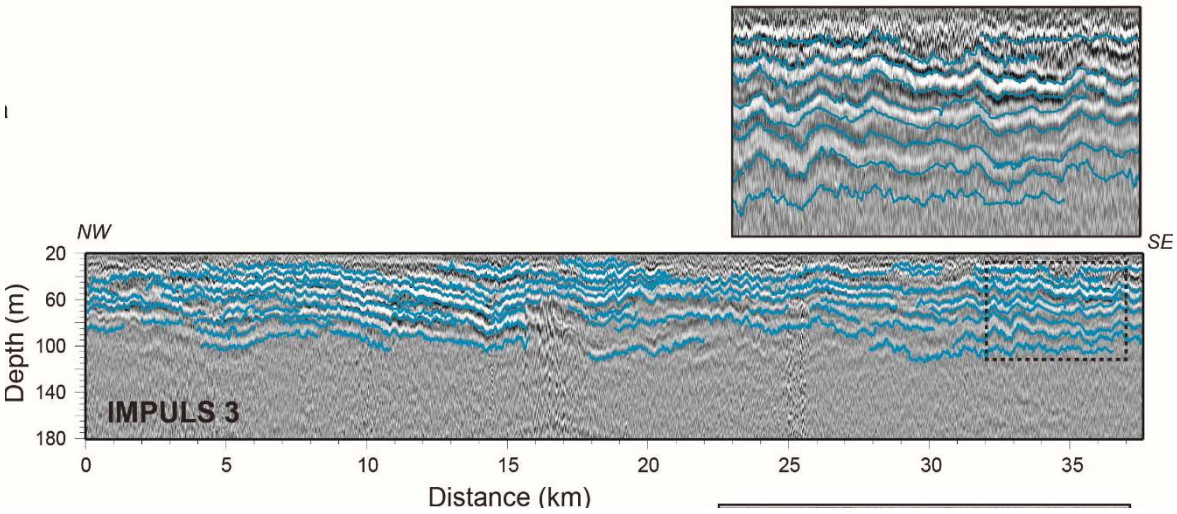

Figure rev2-3. Processed and depth-converted HR-MCS images along profile IMPULS-3, with the tracked reflectors used in the spectral analysis superimposed (blue lines). The depth range of the tracked reflectors is 30-100 m. The inset is a zoom over the area encompassed by the dashed rectangles (fig S5 in Sallares et al., 2016).

At this sub-mesoscale (~window size) we apply the Gregg89 approach (Gregg, 1989), which considers the Garret-Munk model (Garret and Munk, 1979). The observations agree with the model predictions sufficiently well to assume that it describes the link between internal waves and turbulence. The interpretation is that the model is close enough to reality to capture the principal interactions scaling the turbulent dissipation in the thermocline (line 162-165).

Second, slope spectra rely on the aggregate data of many tracks to have statistically characteristic behaviors (Klymak and Moum, 2007 part II). All of what we are shown are single-track spectra.

Several single-track spectra, as well as the combined spectra of all reflectors for two different seismic profiles including the one analyzed here, are presented in detail in Sallares et al (2016). Both the single and the combined spectra (fig rev2-4) consistently show analogous spectral slopes and slope breaks at the same horizontal scales. Additionally, the spectral slopes coincide with theoretical estimations for three different, well-known sub-regimes: the Garret-Munk model for internal waves at >100 m, Kelvin-

Helmholtz instabilities at ~100-30 m, and Batchelor model for turbulent regimes (< 30 m) (line 137-141, 150-152).

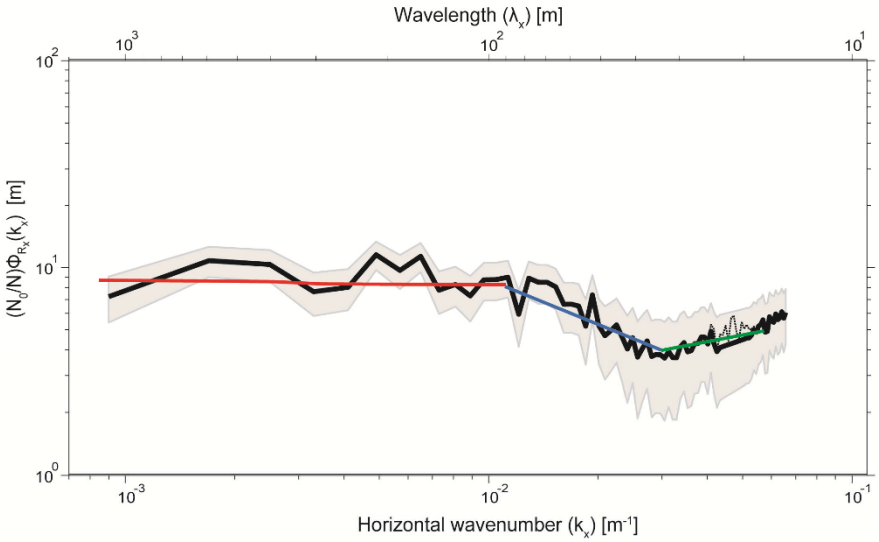

Figure rev2-4. Average horizontal spectrum of the vertical displacement, scaled by the local buoyancy, obtained for the 68 reflectors (solid line) and their corresponding 95% confidence interval (2σ) (shaded area). The reference lines are the theoretical slopes corresponding to the GM79 model for the internal wave subrange (red line), Kelvin-Helmholtz instabilities for the transitional/buoyancy subrange (blue line), and Batchelor59 model for turbulence (green line). The dashed line follows the original, unfiltered part of the spectra in the region affected by harmonic noise arising from repeated shooting. This is eliminated by applying a stop band of 0.027 to 0.021 Hz.

Third, more justification of the horizontal wavenumber bounds for the sub-regimes (IW, instability/transition, and turbulent) are needed to illustrate these are accurate bounds for sub-regimes all over the 2D line. The authors need to be clearer about the role of basic oceanographic features and the expression of turbulent structures.

This issue is also addressed in Sallares et al (2016). As it can be observed in fig rev2-4, the combined spectra of the 68 spectra show clear slope changes consistent with theoretical estimates for the three sub-regimes referred to above at precise wavenumbers (~100 m and ~30 m, respectively). The bound between the IW and shear instability regimes coincides with $l_N=2\pi\Delta V/N$, where N is the buoyancy frequency, and ΔV is the root mean square amplitude of the velocity fluctuation about the mean, which is also calculated within the targeted depth range (30-110 m) from ADCP data. The same spectral slopes and bounds are also obtained in the other seismic profile analyzed in Sallares et al (2016). This behavior also holds for most of the individual tracks. Note that otherwise we would not obtain such clear trends in the combined spectra (fig rev2-4) (137-141, 152-156).

Our interpretation in Sallares et al. (2016) is that the energy cascade between internal waves and turbulence at the sheared thermocline presents a distinct transitional subrange, possibly governed by vortex sheet dynamics. We suggest that the transition starts with the inset of shear instability along the stratified thermocline, follows with the development and rollup of KH billows, and ends with their breaking, collapse and dissipation. The energy needed to maintain these spectra comes from internal waves generated by tidal forcing at the Gibraltar strait, which are in turn subjected to a constant shear between the Atlantic and Mediterranean waters. Even though our analysis is local, the fact that the individual spectra display systematically the same transitional subrange at about the same scales, strongly suggests that this chain of processes is occurring continuously and simultaneous over the whole surveyed area (lines 150-152).

Lines 245-246 state “there is no clear visual correspondence between the k anomalies and the most obvious of the imaged oceanographic features such as IWs” which seems to be against the main thrust of the paper that sub-mesoscale features can be examined through their turbulent expressions, particularly lines 19-21 in the abstract as well as a few points in section 4.

We do not refer to all sub-mesoscale structures “in general”, but just to the internal waves that affect this region. The variations in diapycnal diffusivity show no clear correspondence with internal waves, but rather with the shear instability-like features identified in the transitional range between 100-30m (figures 7-8). We have modified the text to clarify this (line 19-21, 248-250, 339-341).

The manuscript thesis is about ocean mixing, as such, the turbulent subrange should be examined for tracks H1 and H2. Perhaps there are corresponding traits between the IW subrange and turbulent subrange, or the transitional subrange and turbulent subrange that may clarify the expression of turbulence by mesoscale and sub-mesoscale oceanographic features. Uncertainties are problematic and under addressed.

Thanks for the recommendation. We do agree and, in fact, we already examined the turbulent subrange to check if there was any correspondence between the features observed in this subrange (<30 m) and in the other two, and with the location of “mixing hotspots”. We show two examples for H1 and H2 in figures rev2-5 and 2-6, respectively. It appears that it could be (fig rev2-5d), but the problem is that this subrange is too close to the resolution limit, especially in the vertical dimension of the analyzed structures, so data are rather noisy and it does not allow extracting meaningful conclusions.

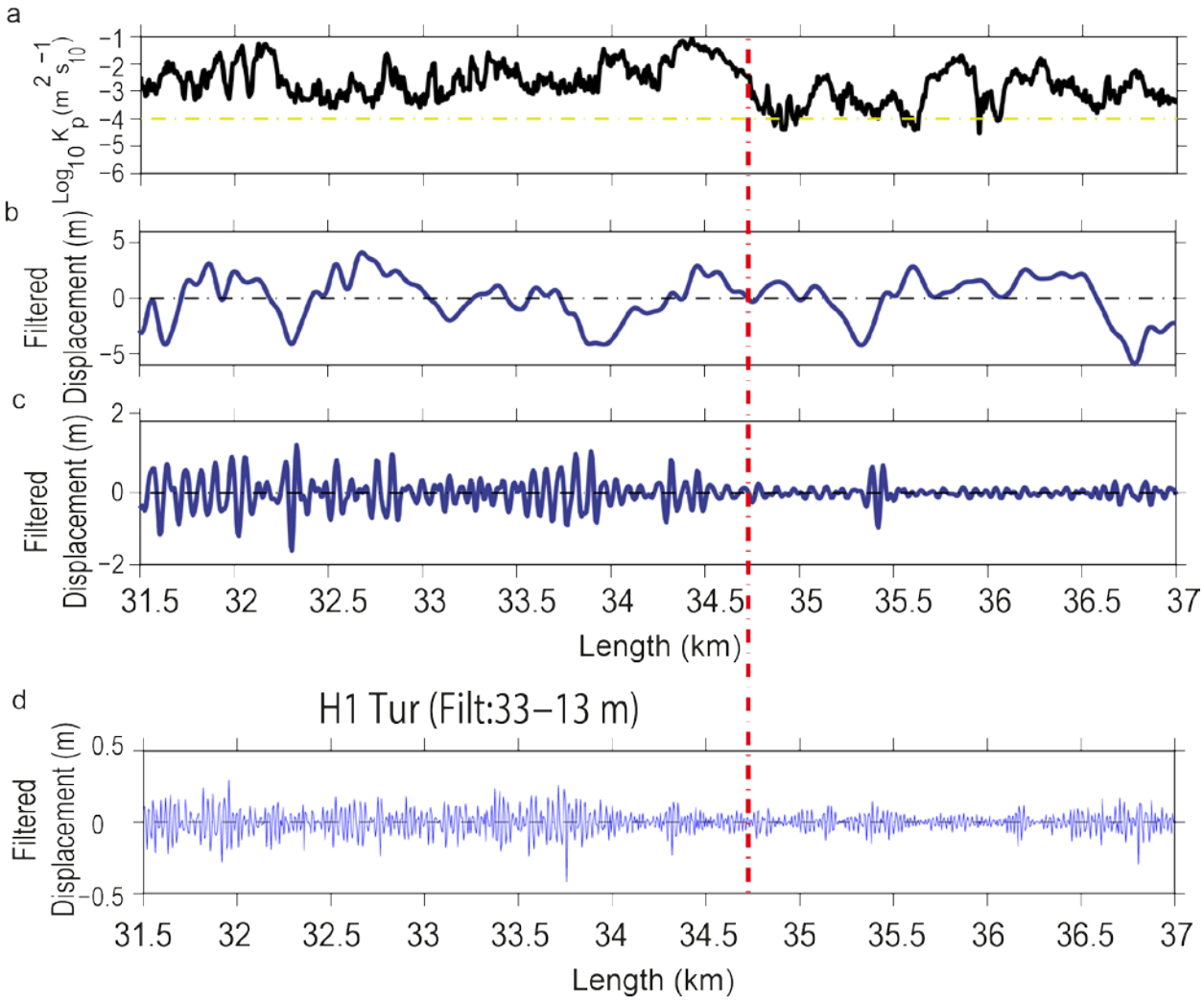

Figure rev2-5. (a) Diapycnal mixing obtained along H1 (see details of calculation in the text). (b) Signal filtered at wavelength ranges of the IW sub-range (*3000-100 m*), (c) the transitional subrange (*100-33 m*), (d) and the turbulence subrange (33-13 m). The dashed red line identifies the "breaking point" referred to in the text.

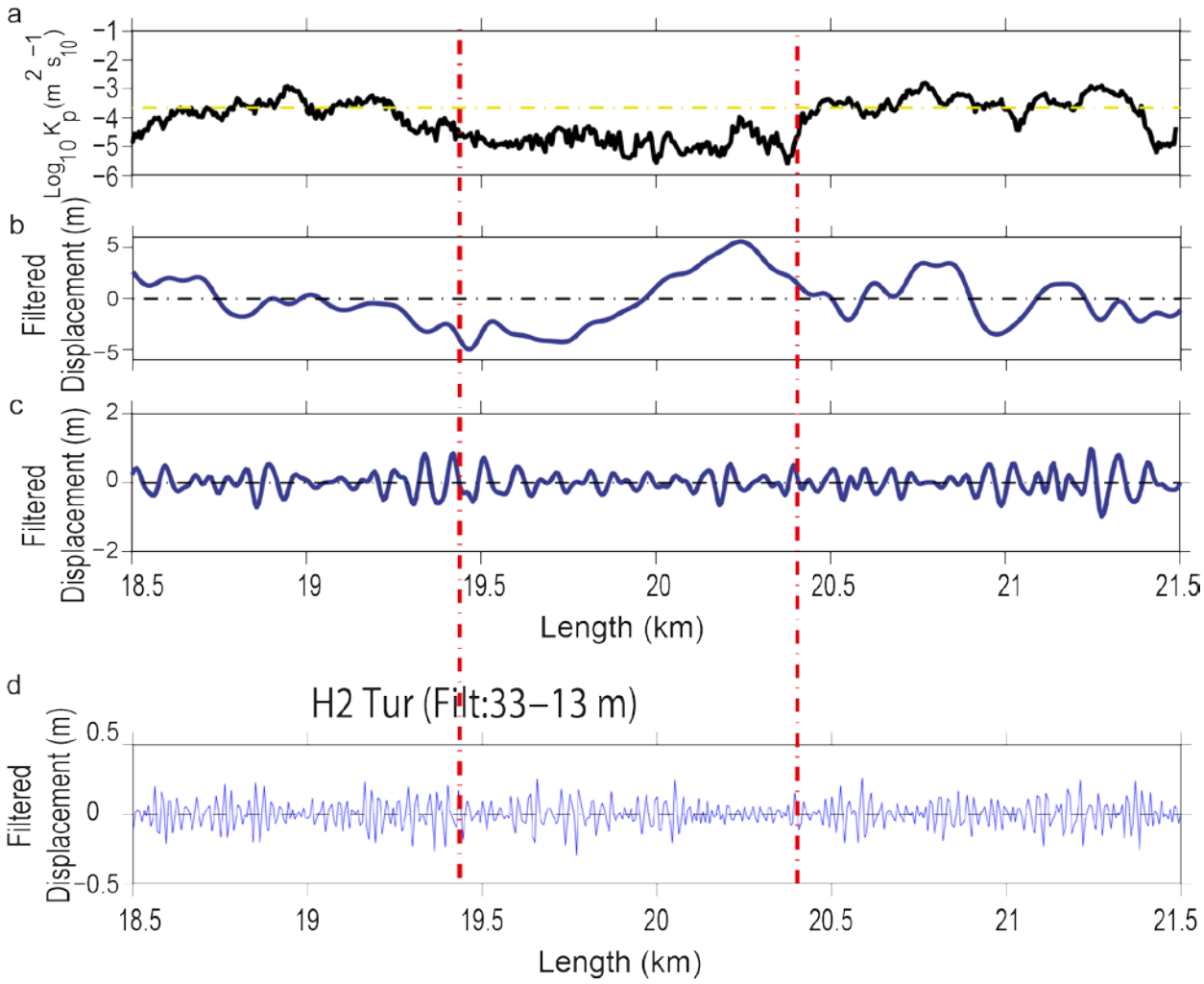

Figure rev2-6. (a) Diapycnal mixing obtained along H2 (see details of calculation in the text). (b) Signal filtered at wavelength ranges of the IW sub-range (*3000-100 m*), (c) the transitional subrange (*100-33 m*), (d) and the turbulence subrange (33-13 m). The dashed red line identifies the "breaking point" referred to in the text.

In the abstract (line 23) and conclusion (line 372) results are stated to be within uncertainty bounds but nowhere in the data do the authors show or discuss any uncertainty assessments. In section 3.2 uncertainty is briefly mentioned, but again, is simply stated that values are within uncertainty bounds. If the conclusions are supported within an uncertainty range, please show and elaborate.

Saying that the results agree "within uncertainty bounds" was an overstatement from our side. We have changed this in the new version. What we actually meant is that the global average and the values obtained with the XCTD are "within the range of values" obtained from the seismic data analysis (compare figs 4 and 5). We have reworded the text accordingly (line 22-24, 376-379).

The major conclusions for the filtered spectra analysis are under supported. Lines 378-381 deliver major conclusions about the relationship between IWs and overturning as well as shear instabilities and mixing hotspots. From the data presented, it appears these conclusions are drawn from the analysis of 2 tracked seismic reflections, H1 and H2. This overstates what is observed in the data, particularly when those two tracks were chosen as end-member individuals chosen for their position in “anomalously high (H1) and low (H2) mixing patches” (lines 264-265).

Thanks for the comment. First, we agree that the relationship between IWs and overturning is unclear and not directly justified by our results, so we have dropped this part from the text. Second, the relationship between shear instabilities and mixing hotspots comes from the analysis of various reflectors, not just H1 and H2. Here we show another reflector (H4) that show a similar pattern to H1. What we actually see is a correspondence between areas showing high diapycnal diffusivity and the location of the largest-amplitude features in the transitional domain, which we interpret to correspond to shear instabilities (possibly KH billows) based -also- on the results of Sallares et al. (2016). We have reworded lines 260-263 to clarify this.

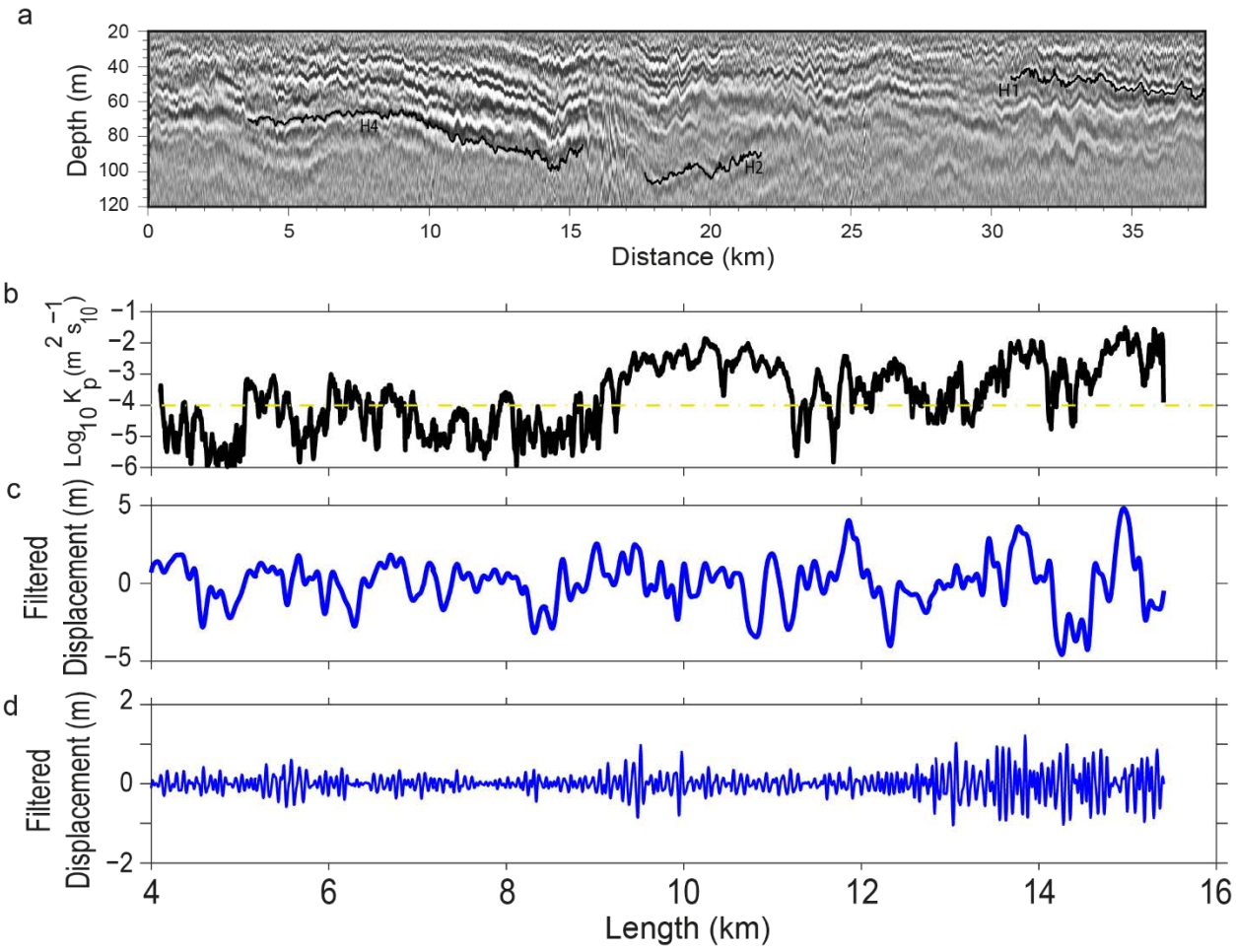

Figure rev2-7. (a) Location of H4 reflector. (b) Diapycnal mixing obtained along H4. (c) Signal filtered at wavelength ranges of the IW sub-range (*3000-100 m*), (d) the transitional subrange (*100-33 m*).

General Comments: The manuscript thesis states that authors produce a map of diapycnal mixing that show patchy nature. However, they often refer to an average k as a benchmark to compare to conventional methods. The authors need to discuss why they would average the entire map when the main thrust of the paper is that it is heterogeneous.

The average k_ρ values presented in figure 4a is just a reference to compare with the range of values that we obtain from the seismic data. This way we confirm that our values are consistent with the ones inferred using more conventional oceanographic methods (same order of magnitude). But we fully agree that the main point of our results is the patchy nature and the range of variability (of over 4 orders of magnitude) in k_ρ. In this sense, we agree that the mean MCS/XCTD values shown in fig 4 were misleading so we have deleted them and we have incorporated instead a shadowed rectangle indicating the range of values obtained in the maps, which coincide with the range of values obtained from the XCTD (new figure 4).

Additionally, the authors need to justify why just 1 XCTD and 1 ADCP data set would accurately reflect the average for their produced mixing map. For example, even if the XCTD was collected concurrently, what would the implication be if it was dropped at 8 km where k is high, or at 22.5 km where k is low?

We agree that the hydrographic data are limited. However, these are the only "quasi-synoptical" data that we have, and we think that it is valuable to incorporate them in the discussion. The fact that both the average values for the whole column as well as the range of variability obtained from the XCTD compare well with those obtained from the –completely independent- seismic data is, in our opinion, a relevant result that is worth mentioning.

Please explain how signal-to-noise is calculated. A signal-to-noise ratio of higher than 8 with 6-fold data is surprising.

As it is explained in Sallares et al. (2016), an important step towards the calculation of the slope spectra is to suppress the random noise from the data and concentrate the analysis in the frequency bands where signal is clear. This can be efficiently done by: (1) estimating the signal-to-noise ratio (S/N) in the different frequency bands, and (2) selecting and applying a band-pass frequency filter that maximizes S/N. To estimate S/N we have applied a cross-correlation-based analysis that consists of the following steps:

i) Band-pass filtering the data;

ii) Calculate the cross-correlation (CC) between each seismic trace and all its

neighbors within a distance equal to the length of the shortest reflectors used in the spectral analysis, d_{CC}=1,250 m. This is first done in the upper part of the profile (30-120 m), hence the section that we consider to contain the signal.

iii) Calculate the maximum value of the CC within a time window corresponding to the mean separation between contiguous reflectors, t_{CC} =10 ms, for each couple of traces (*MaxSigij*);

iv) Calculate the average value of *MaxSigij* for each seismic trace along the whole profile (*AvMaxSigi*);

v) Repeat steps ii) to iv) for the bottom part of the profile (120-240 m), which we consider to be noise, to obtain *AvMaxNoisei*;

vi) Calculate the ratio *S/Ni=AvMaxSigi/AvMaxNoisei* for each seismic trace;

vii) Calculate the average value of *S/Ni* for all the seismic traces: < *S/Ni*>=S/N;

viii) Repeat steps i) to vii) for the next frequency band.

Much of section 3 (first paragraph) should be expanded and put into section 2

Ok, we have done this.

Please explain why tracks H1 and H2 were analyzed with 1 km windows when the turbulent maps were analyzed with 1.2 km windows. The difference in these windows change the wavenumber range of the IW spectra and might aid some of the confusion around the handling of internal waves in the manuscript.

It was a typo. The window size for H1 and H2 is the same as in the map (1.2 km-wide) (line 272, 299).

Further, why limit the analysis to ~1 km? If they exist, larger IWs should carry even more energy and may be important.

At the spatial scale where we focus the analysis, the variation induced at longest wavelength does not affect directly the transitional subrange, as we confirm in figure rev2-2

At many points the authors state there are “no clear correlation” or similar language between filtered spectra (e.g. lines 287, 329-331). Were correlations and statistics taken for each of the 68 tracked reflectors to support, or not, a relationship between the filtered spectra? If so, this should be a major point of the paper and have supporting figures.

No, we have not formally analyzed the statistical correlation between different signals. What we mean is that there is a visual correspondence between different features, as it happens, e.g., between high values of diapycnal mixing and large-amplitude features in

the transitional domain. We have changed the word “correlation” by less confusing ones as “visual correspondence”, or similar, in the new version of the manuscript (line 292, 336, 383).

In figure 6, please show the actual fit lines for these data. This would allow for a brief discussion in the text of how you calculate spectral energy levels beyond a reference to Sallares et al. 2016.

We have modified the figure caption and text as suggested to briefly describe the procedure as follows: Figure 6 shows the average horizontal spectrum of the vertical displacement of tracked reflectors ($\Phi\varsigma_x$) scaled by the local buoyancy frequency at the reflector depth (N/N_0) to eliminate stratification effects, and multiplied by $(2\pi k_x)^2$ to enhance slope variations (blackline). The reference lines are theoretical slopes of Garrett-Munk internal wave model [Garret and Munk, 1979] (red line), Kelvin-Helmholtz instabilities [Waite, 2011] (blue line), and Batchelor's model for turbulence [Batchelor, 1959] (green line).

Specific comments:

Line 85: Citation should be Holbrook et al., 2003.

Done

Line 175: Authors need to state and explain their choice for b the scale factor

It is the scale depth of the thermocline, where we focus the analysis and where we identified the internal waves.

Lines 329-330: Suggest rewording. The authors infer IW-induced mixing is not efficient enough to keep the overturning in this dataset, I do not think the data shown makes it clear, particularly on a global scale.

Reworded to reflect better the results.

Line 340: Suggest rewording. A smooth seafloor likely suggests a lesser role in the generation of hotspot mixing, if it is disregarded entirely, please explain.

Done

High-resolution diapycnal mixing map of the Alboran Sea thermocline from seismic reflection images

Jhon F. Mojica[1-2], Valentí Sallares[2], Berta Biescas[2-3]

[1] Center for Global Sea Level Change – NYUAD, Abu Dhabi UAE.
[2] Institute of Marine Sciences-CSIC, Barcelona, Spain
[3] Consiglio Nazionale delle Ricerche-ISMAR, Bologna, Italy

Correspondence to: Jhon F. Mojica (jfm11@nyu.edu)

Abstract. The Alboran Sea is a dynamically active region where the salty and warm Mediterranean water first encounters the incoming milder and cooler Atlantic water. The interaction between these two water masses originates a set of sub-mesoscale structures and a complex sequence of processes that entail mixing close to the thermocline. Here we present a high-resolution map of the diapycnal diffusivity around the thermocline depth obtained using acoustic data recorded with a high-resolution multichannel seismic system. The map reveals a patchy thermocline, with areas of strong diapycnal mixing juxtaposed with others of weaker mixing. The patch size is of a few km~~s~~ in the horizontal scale and of 10-15 m in the vertical one. The comparison of the obtained maps with the original acoustic images shows that ~~vigorous~~ mixing tends to ~~occur~~ concentrate in areas ~~of~~ where internal wave become unstable and shear instability~~y~~ies develop ~~, whereas mixing levels in more stable areas is lower~~. These results are also compared with others obtained using conventional probes. The values estimated~~obtained using the two methods agree~~ based on the seismic data are within the ranges of values obtained from oceanographic data ~~-~~analysis~~uncertainty bounds~~, and they are also consistent with reference theoretical values. Overall, our results demonstrate that high-resolution seismic systems allow to remotely quantify mixing at the thermocline depth with a lateral resolution of O(10^1 m).

KEYWORDS: Thermocline mixing, Seismic Oceanography, Diapycnal diffusivity map.

1. INTRODUCTION

Diapycnal diffusivity (k_ρ) around the thermocline plays a major role to control the strength and pattern of the ocean circulation, because it determines heat and salt heterogeneity at different spatial scales. This process usually occurs in a vertically stratified regime, affecting adjacent layers with the same density but different temperature and salinity (Stewart, 2008). In terms of processes, mixing in the ocean can be separated in two categories. One is related to internal wave (IW) breaking, which produces turbulent motion and changes the density stratification; while the second concerns the development of high frequency dynamic instabilities that are formed due to shear (Gregg, 1987; D'Asaro and Lien, 2000~~Laurent and Garrett, 2002~~). As the spatial scale decreases, mixing leads to an unbalanced pressure field that eventually ~~can~~ result~~s~~ in a collapse and dispersion of mixing waters through isopycnals (Thorpe, 2005). The value of k_ρ depends on the buoyancy frequency (N) and the dissipation rate (ε) as indicated by the so-called Osborn (1980) relationship:

$$k_\rho = \Gamma \varepsilon / N^2 \quad (1)$$

This value, where $\Gamma = 0.2$ is the empirically defined mixing efficiency (Osborn and Cox, 1972), corresponds to the mixing between isopycnal layers in the thermocline. The global mean k_ρ value is of the order of $10^{-4}\ m^2s^{-1}$ (Munk and Wunsch, 1998), which corresponds to the value required to keep overturning in the thermocline. It has been shown that if $k_\rho < 10^{-5}\ m^2s^{-1}$ there is not enough energy to generate mixing (Gregg, 1989).

In a conservative flow, ε might present small variation due dissipated heat through turbulent motions~~If the flow is conservative, ε must be independent of the spatial scale~~, but ~~it might present small variations due to the fact that it involves work against buoyancy, so that mechanical energy is transformed to heat through turbulent motions. I~~in the presence of strong shear, ε tends to increase (Thorpe, 2005), reaching a maximum value close to the Kolmogorov scale (Gargett and Holloway, 1984). Good knowledge of its behavior provides important clues on available energy and its transfer between spatial scales.

The loss rate of kinetic energy in the turbulent motion is commonly expressed as:

$$\varepsilon = \left(\frac{\nu}{2}\right)\langle S_{ij}S_{ij}\rangle \tag{2}$$

$$S_{ij} = \left(\frac{\partial u_i}{\partial x_j} + \frac{\partial u_j}{\partial x_i}\right) \tag{3}$$

Where $\nu = 1.064x10^{-6}\ m^2s^{-1}$ is the kinematic viscosity and the tensor S_{ij} is a function of the velocity components in the three orthogonal directions (Thorpe, 2005). Conventional in-situ techniques as Vertical Microstructure turbulence Profiler (VMP) or microriders provide the most accurate ~~that are commonly used to directly~~ measures of k_ρ, but in just one dimension. ~~have the problem that they are intrusive, in the sense that the measuring itself modifies the mixing levels at the small scales.~~ In general~~addition~~, although measures are accurate in the vertical dimension, sampling in the horizontal direction is much poorer, particularly in the $\sim 10^3$-$10^1\ m$ range (Klymak and Moum, 2007 a, b). Since this is the range of scales at which the transition between isotropic internal wave and anisotropic turbulence motion (i.e. mixing) occurs, the observational evidence of mixing patterns and the understanding of the underlying physical mechanisms are rather limited so far. Overall direct measures and observations are too few to create a global mixing map with the required resolution to feed the models with appropriate dissipation ranges (Smyth et al., 2011). This makes it in turn difficult to integrate mixing into large-scale ocean dynamics models. Its effects are simulated instead through the incorporation of eddy diffusivity coefficients, which are tuned *ad hoc* to match the large-scale distribution of ocean observables. While this approach allows to properly reproduce regional spatial-temporal patterns, it severely hampers the long-term predictive capability of ocean dynamics and, in turn, that of climate models. Improving our knowledge on the short-term and small scale mixing mechanisms and integrating them into large-scale models remain thus as an outstanding challenge.

To overcome this issue, remote sensing techniques have recently started to be used (e.g. Gibson et al., 2007). One of these alternative techniques is ~~the~~ multichannel seismics (MCS)~~ system~~, an acoustic method providing quasi-synoptic images of the thermohaline boundaries in the ocean interior to full ocean depth, with a lateral resolution of up to $\sim 10^1\ m$ (Holbrook et al., 2003~~and Fer, 2005~~). Several recent works have demonstrated that it is actually possible to map k_ρ using measures

of the horizontal wavenumber (k_x) spectra of the vertical displacements of thermohaline boundaries imaged with MCS acquisition systems (Sheen et al., 2009; Holbrook et al., 2013; Fortin et al., 2016). However, these studies use conventional, relatively low resolution ~~MCS acquisition~~ systems with source energy concentrating below *~50 Hz*. In addition, these systems are not well-suited to image the shallowest ocean layers (i.e. < 200 *m*), but deeper water levels (≥ 400 *m* depth). At these depth levels, the changes in the internal structure are usually less marked than those at shallower levels, and especially around the thermocline. In a recent work, ~~Sallares et al. (2016)~~it has been shown~~ed~~ that high resolution MCS (HR-MCS) systems, which use a small energy, but~~and~~ higher-frequency source, allow imaging the thermohaline structure as shallow as *~30 m* with a lateral resolution of *12-~~~15 m* and *1-~2 m* in the vertical direction (Sallares et al., 2016). This resolution is three- to four-fold better than that of conventional MCS systems used to image~~at~~ deeper ocean levels. Therefore, it has the potential to image sub-mesoscale structures and processes that affect the thermocline at scales of kilometers to tens of meters, allowing ~~therefore contributing~~ to cover the existing observational gap. Despite its potential, HR-MCS systems have never been used to date to quantify diapycnal mixing at the thermocline depth.

Here we use the above-mentioned method of extracting $k_\rho(x, z)$ maps from MCS images, ~~(Sheen et al., 2009; Holbrook et al., 2013),~~ but applied for the first time to HR-MCS data acquired in the Alboran Sea (Westernmost Mediterranean). The method to calculate diapycnal mixing maps from the horizontal wavenumber spectra of vertical reflector displacements is analogous to that proposed by Sheen et al. (2009) and Holbrook et al. (2013). The result is a high-resolution mixing map of the ocean at the thermocline depth (*30-15~~5~~10 m*) along a *35 km*-long transect (Fig. 1a). This method can be used in other regions where the water column is sufficiently stratified to record the acoustic impedance variations (density x sound speed contrasts between neighboring water layers).

The rest of the manuscript is structured as follows: in section 2 we present the hydrographic context, and the observations; then we describe the acquisition system and the method applied to estimate k_ρ from the seismic data. The results are described in section 3, whereas the discussion about the imaged structures and their likely causes is presented in section 4. Finally section 5 summarizes the main conclusions.

2. DATA AND METHODOLOGY

The Alboran Sea is characterized by the continuous exchange between Mediterranean Water (MW) and Atlantic Water (AW) through the Strait of Gibraltar. This exchange concentrates near the surface (between *~30 m* and *200 m*); where the shallow, moderately saline and cold incoming AW (< 50 *m*) interacts with the deeper, warmer, saltier and more stable outgoing MW, producing another water mass known~~referred to~~ as Modified Atlantic Water (MAW). In this framework, internal waves, strong horizontal shear instability, and prominent thermohaline stratification are generated. These particular features reflect the complex dynamic setting of the area, with kinetic energy being transferred between isopycnals from large to small scales, leading eventually to overturning, isotropic turbulence and irreversible mixing.

The data set used in this work, which includes collocated seismic and oceanographic measurements, was collected in the framework of the IMPULS-2006 experiment. Here, we

concentrate our analysis on one of the seismic profiles (IMPULS-3), which was acquired on board the Spanish R/V Hesperides using a HR-MCS system. The acquisition started on May 16th at 23:43 and finished on May 17th at 04:00. In total, some 4 hours to record a 38 km-long profile. The acquisition system consisted of a 4.75 liters source with a peak frequency at 150-190 Hz. The corresponding size of the Fresnel zone, a proxy of the horizontal resolution (e.g. Sheriff and Geldart, 1995), is ~~*12-*~~*15 m*. The streamer was 300 m-long and had 48 channels, with a group spacing of 6.25 m. The shot interval was 15 m, giving a Common Mid-Point (CMP) gathers ~~(Yilmaz and Doherty, 1987)~~ fold of 6. The location of the different data is displayed in Fig. 1a.

This profile was first processed and used to estimate the k_x energy spectra of the vertical displacements of the seismic reflectors ~~(Sallares et al., 2016)~~. A total of 68 reflectors were tracked and used for the analysis (Sallares et al., 2016). As it is shown in this paper, the 68 reflectors are rather homogeneously distributed throughout the analyzed area, they have ~~with~~ lengths of *1.5-21 km*, and a signal-to-noise ratio higher than *8* within the frequency range of *40–240 Hz* ~~were identified and used for the analysis~~. Vertical profiles of temperature and pressure were recorded simultaneously with the seismic acquisition using 4 XBT's; whereas the salinity and buoyancy profiles were obtained from an XCTD, dropped three days after the seismic acquisition. Water current profiles have also been used in the study, but they are not coincident with the seismic acquisition (see location in Fig. 1a). They were obtained during the SAGAS experiment on board the Spanish R/V Sarmiento de Gamboa using an ADCP ocean surveyor 75, in the same season as the seismic experiment but 4 years later.

The HR-MCS profile shown in Fig. 2 reveals a number of laterally coherent seismic reflectors that are assumed to follow isopycnals (Biescas et al., 2014). The analysis of the obtained k_x spectra allowed identifying three sub-ranges that control dynamics around the thermocline depth at increasingly small spatial scales (Sallares et al., 2016). Thus at scales larger than the horizontal buoyancy wavelength ($l_N \approx 90$ *m*), motions are dominated by the internal wave field (internal wave-field subrange); then the spectra rolls off reflecting the presence of shear instabilities of probably the Kelvin-Helmholtz (KH) type, which appear to collapse at a scale of *~30 m* (transitional or instability-dominated subrange), giving rise to turbulence at even smaller scales (turbulent subrange). A more detailed description of these ranges and their scales is presented in Sallares et al. (2016). In the present work, we use the energy levels obtained from the k_x spectral analysis of the reflectors to estimate the variations of ε and k_ρ along the whole profile.

Since our dataset does not include direct measurements of turbulence, we use the XCTD and ADCP data to estimate a vertical profile of k_ρ based on Gregg's (1989) model; hereafter referred to as Gregg89. The Gregg89 model assumes that energy dissipation in the thermocline is made through IW energy transfer by wave-wave interaction. This model links shear current at different depths The simplest way to obtain average dissipation rates over large space and time scales is through~~as~~:

$$\varepsilon = 7x10^{-10}\, N^2/N_0^2 < S_{10}^4/S_{GM}^4 > \quad (4)$$

$$S_{10}^4 = 4.22[(\Delta U/\Delta z)^2 + (\Delta V/\Delta z)^2]^2 \quad (5)$$

$$S_{GM}^4 = 2[(3\,\pi/2) j_x E_{GM} b N_0^2 k^c (N/N_0)^2]^2 \quad (6)$$

Where $N_0=5.2\ x10^{-3}\ s^{-1}$ is the reference buoyancy frequency, S_{10} is the shear variance calculated from the meridional (V) and zonal (U) velocity variations according to the depth (Z), and S_{GM} is the variance for the Garret-Munk model (Gregg, 1989), where j_x is a mode number, E_{GM} is the Garrett-Munk energy density, b is a scale factor, and k is the horizontal wavenumber.

Alternatively, the model proposed by Batchelor (1959); hereafter referred as Batchelor59, estimates k_ρ as a function of the energy transfer from large to small scales in the turbulent regime. This model assumes that the energy exchange from mechanical to caloric due to N and ε can be approximated as:

$$\varphi_\varsigma^T = \left(\frac{4\pi\Gamma}{N^2}\right) C_T \varepsilon_T{}^{2/3} (2\pi k)^{-5/3} \quad (7)$$

Where φ_ς is the energy spectrum of the isopycnals vertical displacement; and C_T is a proportionality constant (Sreenivasan, 1996). We apply this model to estimate the mixing rates over the seismic profiles applying a method proposed and described in previous works, (i.e. Sheen et al., 2009; Holbrook et al., 2013). The main steps of this approach are described below. ~~These two models are then used to compare and analyze the mixing behavior in the water column.~~

To identify the dissipation signature in the seismic profile, we first calculate the energy level in the turbulent subrange from our data by averaging the value obtained for all reflectors within ~~a~~ 1200 m-wide and 15 m-high windows. Longer tracks are cut to fit inside the window. As it is explained in Sallares et al. (2016), this does not affect the spectrum at the spatial scale range analyzed. We then apply Batchelor59 model, Eq. (7), to estimate ε using the obtained energy level within the window (transitional subrange), with $\Gamma=0.2$, $C_T=0.3$ and N is calculated according to depth. Finally, we apply Eq. (1) using the $\varepsilon(x, z)$ values obtained above to estimate $k_\rho(x, z)$. These steps are repeated within ~~a sliding~~ windows of the size mentioned above that slide~~moves~~ *30 m* in the horizontal direction and *3 m* in the vertical ~~one~~ at eachnew analyzing step ~~along the seismic profile~~. The fact that we incorporate few new data at each step, produces a smoothly varying map instead of the one with sharp bounds that would be obtained without overlapping windows (e.g. Sheen et al., 2009; Holbrook et al., 2013).

In summary, both ~~models~~ Gregg89 and Batchelor59 models~~,~~ are used to estimate ~~the~~ mixing rates from two independent data sets: XCTD-ADCP and seismic data, respectively. The r~~R~~esults obtained using both models are then compared to gain confidence in the proposed methodology. We then analyze and discuss the high resolution 2D map resulting from the seismic data in terms of mixing.

3. RESULTS

~~To identify the dissipation signature in the seismic profile, we first calculate the energy level in the turbulent subrange from our data by averaging the value obtained for all reflectors within a 1200 m-wide and 15 m-high window. We then apply Batchelor59 model, Eq. (7), to estimate ε using the obtained energy level within the window, with $\Gamma=0.2$, $C_T=0.3$ and N according to depth.~~

~~Finally, we apply Eq. (1) using the $\varepsilon(x, z)$ values obtained above to estimate $k_\rho(x, z)$. These steps are repeated within a sliding window that moves 30 m in the horizontal direction and 3 m in the vertical one at each step along the seismic profile.~~ A~~s a result we obtain a~~ smoothly varying k_ρ map that covers the whole profile (Fig. 3) were obtained applying the sliding window approach explained above. ~~The resolution of the obtained map is therefore of ~30 m in the horizontal and ~3 m in the vertical, safe enough given the theoretical limit of the size of the Fresnel zone (~15 m) in the lateral direction, and of the Rayleigh criterion of λ/4 (~2 m) in the vertical one.~~ The goal is being able to identify features and processes occurring in the transition between the internal wave and the turbulence sub-regimes, such as the intensity and scales of variability of the mixing patches, the location and size of the hotspots and their potential relationship with oceanographic features such as IWs or shear instabilities.

3.1. Probe-based $k_\rho(z)$ profile

To have a reference value to compare with the MCS-based $k_\rho(x,z)$ maps, we have first calculated a $k_\rho(z)$ profile for shallow waters (< 200 m) using the XCTD and ADCP data and applying the Gregg89 model (Eqs. 4-6). To do this we have used ADCP measures averaged within 10 m-depth bins. By doing this, we obtain an average value for the shear variance of $S^4_{10} = 0.28\ s^{-1}$, whereas the reference value of the shear variance obtained from the Garrett-Munk model (Gregg, 1989) is $S^4_{GM} = 0.013\ s^{-1}$. This gives an average dissipation rate $\langle\varepsilon\rangle \approx 1.3x10^{-8}\ Wkg^{-1}$, and an average diapycnal diffusivity $\langle k_\rho \rangle \approx 10^{-3.0}\ m^2s^{-1}$ for the targeted depth range (Fig. 4a). The $k_\rho(z)$ profile obtained from the XCTD and ADCP is also shown in Fig. 4a, together with the global averages for overturning ($\langle k_\rho \rangle \approx 10^{-4}\ m^2s^{-1}$) as well as the average pelagic diffusivity in the ocean ($\langle k_\rho \rangle \approx 10^{-5}\ m^2s^{-1}$).

We obtain minimum values of the mixing rate at *50-55 m*, *68-73 m*, and *100-125 m*. The absolute minimum of $k_\rho = 10^{-5.2}\ m^2s^{-1}$ is obtained at *~115 m*~~.~~, whereas the maximum is of $10^{-2.1}\ m^2s^{-1}$ at ~15 m. This gives a range of variation of $10^{-3.1}\ m^2s^{-1}$. Deeper than this, the mixing variability is smaller. The Turner angle and buoyancy frequency (Fig. 4b) indicate that the region is mostly stable with a slight tendency to double-diffusion (*Tu~45°*).

It is worth noting that, at this specific location, the average vertical $\varepsilon(z)$ and $k_\rho(z)$ values are one order of magnitude higher that the global average ones. The higher values probably reflect the effect of overturning in the thermocline. While probe-based measurements are well-suited to investigate mixing variability in the vertical dimension, they do not provide information on the variability in the horizontal dimension with a comparable level of detail. As explained above, to do this we have used estimations of ε and k_ρ based on the HR-MCS data, but applying Batchelor59 model (Eq. 7) in this case.

3.2. High-resolution multichannel seismics-based $k_\rho(x, z)$ map

The $k_\rho(x, z)$ map displayed in Fig. 3 has average values of $\langle\varepsilon\rangle \approx 6.5x10^{-9}\ Wkg^{-1}$ and $\langle k_\rho \rangle \approx 10^{-2.7}\ m^2s^{-1}$. These values are ~~comparable,~~ within the range of values ~~uncertainty bounds, to those~~ obtained from the XCTD and ADCP data but, at the same time, they are over an order of magnitude higher than the global ocean reference value of ~~-~~$k_\rho \approx 10^{-4.0}\ m^2s^{-1}$ (Fig. 4a).

Figure 5 displays the $k_\rho(x, z)$ map superimposed with the HR-MCS data. It is interesting to note that the range of horizontal variability is similar to that observed in the vertical dimension, although there is no direct ~~clear~~ visual correspondence between the k_ρ anomalies and ~~the most obvious of the imaged oceanographic features such as~~ IWs. The range of variability is of over three orders of magnitude, locally reaching an extreme value of $k_\rho \approx 10^{-1.5}\ m^2 s^{-1}$ at a depth of ~*55 m* and at *16 km* along the line; and a minimum value of $k_\rho \approx 10^{-4.5}\ m^2 s^{-1}$ at ~*95 m* depth and *20 km* along the line, which is close to the global oceanic average. Numerous patches with k_ρ values exceeding $10^{-2}\ m^2 s^{-1}$ with a characteristic size of *1-2 kms* in the horizontal dimension and ~*10 m.* in the vertical are found throughout the whole section (i.e., yellowish patches~~anomalies~~ in Figs. 3 and 5). Not only the average depth value, but also the vertical size of the anomalies, as well as the range of k_ρ variation, are in agreement with the probe-based values (Fig. 4). The contribution of the high k_ρ patches to the local average is outstanding, raising it from a background average value of $\sim 10^{-4}\ m^2 s^{-1}$ to $\sim 10^{-2.5}\ m^2 s^{-1}$.

To try to understand the existing relationships between mixing variability and water dynamics, we analyze various reflectors to identify a possible visual correspondence between individual sub-mesoscale features and mixing hotspots. Among the numerous ~~have chosen two~~ horizons examined, we show in fig. 5, three horizons named H1, H2, H3, which ~~that~~ spatially coincide with anomalously high ~~(H1)~~ and low ~~(H2)~~ mixing patches. For these three horizons ~~, and~~ we have ~~individually~~ analyzed the structures observed in the different sub-regimes.

3.3 Analysis of individual reflectors~~a high dissipation area (H1)~~

H1 is located at ~*50 m* depth and has a length of ~*5.5 km* (*31.5-37 km* along profile). It was selected because it is laterally coherent for several kms and, it also coincides with one of the high mixing hotspots (Fig. 5). Its corresponding k_x spectrum is displayed in Fig. 6a.

To calculate k_ρ over the whole horizon (Fig. 7a) we used the spectral energy obtained within a *1.2 km*-wide window moving laterally *30 m* at each step along the whole profile. ~~The estimated average value for the whole H1 is $k_\rho \approx 10^{-2.6}\ m^2 s^{-1}$.~~ To analyze the features that contribute to the energy spectrum in the different scales, and to compare them in turn with the k_ρ values obtained along the entire reflector length, the horizon has been filtered at wavelength bands attributed to the ~~subranges dominated by IW~~internal waves subrange (*3000-100 m*~~, IW subrange~~), and the instability dominated subrange ~~shear instabilities~~ (*100-30 m*~~-33 m~~, transitional subrange). ~~(Sallares et al., 2016).~~ As a reference, the local horizontal buoyancy wavelength, estimated from the XCTD data is $l_N \approx 90\ m$ (Sallares et al., 2016)~~.~~. The different spectral subranges that are observed in the combined spectrum of the 68 reflectors (fig. S1) is also observed in most individual spectra such as those displayed ~~can be seen~~ in ~~F~~fig. 6a~~., where~~ ~~o~~One of the main features is the systematic steep slope spectra at the ~~intermediate scale (~~instability-dominated subrange, which~~ies) that~~ is likely associated with the loss of energy in the wave field due to dissipation (e.g. Samodurov et al., 1995). As it is explained in Sallares et al. (2016), t~~T~~he variation of the slope spectra at the intermediate scale is consistent~~involves a direct relation~~ with numerical estimates for the evolutionary stage of the vortex sheet linked to shear instabilities (Waite, 2011).

A striking feature is the notable, sudden decrease in the amplitude of the features observed in the transitional subrange at ~*34.7* km along the profile (red dashed line in Fig. 7). Interestingly, a change in the k_ρ value is also observed at this point. Left of it (*31.5-34.7 km* along profile), the average k_ρ value is $10^{-2.5}$ m^2s^{-1}, while right of this point (*34.7-37 km*), it is $10^{-3.0}$ m^2s^{-1}. Although both values are higher than the average global value for meridional overturning circulation, the highest local average values are obtained in the region where the clearest, largest amplitude features~~,~~ possibly representing KH billows (Sallares et al., 2016), are imaged. Conversely, there is no clear visual correlation between internal wave ~~amplitude~~attributes and k_ρ variations.

~~3.4 Analysis of a low dissipation area (H2)~~

H2 is located at ~*95 m* depth and has a length of ~*4.0 km* (*18-22 km* along profile). It was selected because its location coincides with a relatively weak mixing area, according to the k_ρ map (Fig. 5). The corresponding k_x spectrum is shown in Fig. 6b. As in the previous case, we have first calculated k_ρ using the spectral energy values within *1 km*-wide window, moving laterally *30 m* at each step, along the whole reflector length. The average value for the whole horizon is $k_\rho \approx 10^{-4.1}$ m^2s^{-1}, so considerably lower than in H1 but close to the global average value. We have subsequently filtered H2 at the IW (*3000-100 m*) and transitional (*100-3~~3~~0 m*) sub-ranges and compared it with the obtained k_ρ values (Fig. 8). In this case, we have identified three different segments as a function of their average k_ρ value. The first and third segments (*18-19.6 km* and *20.4-22 km*, respectively) display average k_ρ values that coincide, within error bounds, with those of the global ocean average. In particular, we obtain $k_\rho \approx 10^{-4.0}$ m^2s^{-1}, for the first segment, and $k_\rho \approx 10^{-3.8}$ m^2s^{-1}, for the third one. The second or breaking segment, instead, displays a value of $k_\rho \approx 10^{-4.8}$ m^2s^{-1}, which is well below the global ocean average.

H3 is located at ~*80 m* depth and has a length of ~*12 km* (*3.5-15.5 km* along profile). It was selected because its location pass through low and high mixing areas, according to the k_ρ map (Fig. 5). The k_ρ values along the profile have been calculated following the same approach as for the other two reflectors. Its corresponding k_x spectrum is displayed in Fig. 6c. As in the case of H1, we can identify a clear visual correspondence of high mixing values and the largest-amplitude features imaged in the transitional subrange, but not with IWs. Between 9 *km* and 15.5 *km* along the profile the average k_ρ value is $10^{-2.7}$ m^2s^{-1}, while at the left of it (4-9 *km* along profile) it is $10^{-4.8}$ m^2s^{-1}. The situation is therefore very similar to the case of H1, and the same correspondence is also observed for the other reflectors along the profile, especially for those located in high mixing areas.

4. DISCUSSION

The spatial variability observed along isopycnals based on the spectral analysis of the seismic data allows identifying a number of local features at different evolutionary stages. These features are the manifestation of relevant oceanographic processes, such as ~~breaking~~ IWs at the internal wave sub-range, hydrodynamic instabilities at the transitional sub-range, and turbulence at smaller scales. Those can be identified by the disruption of the finestructure in the seismic image and the high variability or disappearance of some seismic reflectors.

The large~~quick~~ variations observed in the k_ρ vertical profile (Fig. 2), together with the slight tendency to double-diffusion identified in the Turner angle, suggest that the system is prone to be affected by advection processes (e.g. Kunze and Sanford, 1996). Mixing appears to concentrate within the MAW, where the shear values are the highest in the study area, and not deeper than > *110 m*, where there is no remarkable shear and the system is weakly stratified. The shear to strain ratio calculated applying the Gregg89 model ($S_{10}^4/S_{GM}^4 = 21$), indicates that the energy in the IW field is higher than that of the GM model, which usually has a value of 3. We can therefore make the assumption that the energy is distributed in the whole inertial range where the water structures are stable (e.g. Munk, 1981). Similar results were obtained by Holbrook et al.~~,~~ (2013), who registered a shear to strain ratio of *17*. The IWs can therefore be considered as an energy distributor from anisotropic to isotropic motions. The k_ρ value obtained from XCTD and ADCP using Gregg89 model is $k_\rho \approx 10^{-3.0}\ m^2s^{-1}$, whereas we obtain $k_\rho \approx 10^{-2.7} m^2s^{-1}$ using MCS data and the Batchelor59 model. The range of variation in the two cases are also comparable, being the maximum values of $10^{-2.2} m^2s^{-1}$ and $10^{-1.5} m^2s^{-1}$, and the minimum values of $10^{-5.4} m^2s^{-1}$ and $10^{-5.7} m^2s^{-1}$, respectively, for the two methods. These similar values obtained based on different models and using independent techniques are well above the global average, suggesting that the energy transfer to small scales is highly efficient in the studied area.

We find~~ound~~ no direct correlation between the presence of IWs and k_ρ. Thus, we interpret that IW-induced mixing is ~~clearly~~ not efficient enough to keep the overturning in the target area (Figs. 7 and 8). No clear correspondence~~lation~~ between IW amplitude and k_ρ variation is found along any of the three ~~H1 and H2~~ reflectors. This lack of correlation agrees with Klymak and Moum (2007 a) assumption, suggesting a weak dependence of mixing rates on IW energy. The mixing rates are more reliably measured ~~in~~at smaller scale regimes, in this case the instability-dominated regime that encloses the ~~-~~transition~~al~~ towards ~~regime to~~ turbulence. In our case, a number of "mixing patches" have been identified at specific locations in the k_ρ map (Fig. 3), which appear to spatially coincide with areas where shear ~~of IW~~ instability features are located (see reflectors H1 and H3 in figs. 7, 9). These mixing hotspots likely represent a significant source of regional diapycnal mixing at the boundary layer between the MAW and the MW (*30 – 200 m*), which is subject to vertical stratification and shear values of $3.2x10^{-3}\ s^{-1}$. The mixing and energy transfer between these two water masses constitutes the main energy source of the region. The smooth and relatively deep seafloor along the profile (> *800 m* in average; ~~F~~fig. ~~9~~10b), likely suggests a small contribution to the generation of ~~allows discarding~~ mixing hotspots~~. to be a consequence of water-seafloor interaction.~~ Given that the MAW-MW boundary layer is subject to shear (Fig. ~~9~~10a), and taking into account the visual correspondence between the location of the largest amplitude features in the instability-dominated domain and high mixing values, we hypothesize that the direct cause of mixing hotspots is the development of IW shear instabilities. This could explain both the peak values of k_ρ and the high variability along the profile.

The k_ρ values along H1 are over the global average for overturning along most of the reflector ($\langle k_\rho \rangle \approx 10^{-2.5}\ m^2s^{-1}$), with lower values only at specific points (Fig. 7a). These points are located to the right of 34.7 km, where k_ρ sharply decreases. A similar situation is also observed along H3, reaching a global average ($\langle k_\rho \rangle \approx 10^{-3.1}\ m^2s^{-1}$). The spatial correspondence between high diffusivity values and the presence of large-amplitude features interpreted to correspond to KH-like shear instabilities by Sallares et al. (2016) ~~billows~~ at the transitional subrange, is consistent with the hypothesis that a causal relationship exists between the two. This is conceptually equivalent to the

mechanism proposed by Gregg (1987), where mixing at the transitional subrange occurs principally at vortex sheets through wave-instability. We could therefore hypothesize that the presence of a vortex sheet left of 34.7 km along profile produces the high mixing values; whereas to the right, there is no vortex sheet and the ocean is more stable. Similar results suggesting a patchy ocean interior, although at larger scales and deeper levels, were also presented by Sheen at al. (2009) and Fortin et al. (2016). Our work confirms these previous results and suggests that the variation is probably due to the high mixing induced by the shear instabilities; which enhances in turn energy transfer to small~~er~~ scales.

5. CONCLUSIONS

We have used acoustic images obtained with a high-resolution MCS system to produce a 2D diapycnal mixing map~~s~~ at the thermocline depth. Our results confirm a high level of diapycnal variability and the presence of marked mixing patches in the water column. The $k_\rho(x, z)$ map obtained by applying the Batchelor59 model to the seismic data, has a strong variability with values ranging between ~~a average~~ $<k_\rho> \approx 10^{-\text{~~1.2~~}1.57} m^2s^{-1}$, in the high mixing patches (hotspots) and $<k_\rho> \approx 10^{-3.3} m^2s^{-1}$, for the background values~~ comparable in both magnitude and range of vertical variability with the value of $<k_\rho> \approx 10^{-3.0} m^2s^{-1}$ obtained applying the Gregg89 model to XCTD and ADCP data~~. The obtained values are high enough to account for overturning at thermocline depths. The mixing hotspots have a characteristic size of *10-15 m* in the vertical dimension, and *1-2 km* in the horizontal one. They are located at different depths within the thermohaline layer, although they appear to concentrate in highly sheared regions. ~~Both the~~The comparable ~~mixing~~ values obtained ~~and the vertical scale of the features imaged~~ with the two independent methods and approaches ~~are consistent within uncertainty bounds;~~ confirm~~ing~~ that HR-MCS is a useful technique to study processes and structures occurring at the sub-mesoscale, which are difficult to be studied otherwise.

The relationship between mixing variability and ocean dynamics at different spatial scales is investigated by analyzing the spectral amplitudes along two seismic horizons in the internal waves and transitional, or instability-dominated, subranges. On ~~the~~ one hand, we found no clear corres~~pondence~~~~lation~~ between the location of the mixing patches and the location~~presence~~ and amplitude of IWs~~, confirming that IWs do not appear to produce overturning~~. Conversely, a visual correspondence exists between the location of shear instabilities and mixing hotspots in different reflectors, suggesting a causal relationship between both features. Areas displaying the most vigorous instabilities coincide with the highest estimated diapycnal mixing values, which are well above the average global value for meridional overturning. This observation suggests that the energy transfer from anisotropic to isotropic scales is highly efficient at thermocline depths within the studied area.

Overall, our study shows that the HR-MCS technique can be used to study sub-mesoscale structures and processes at the thermocline level, provided that the stratification is strong enough to produce acoustic reflectivity that can be recorded by the system. The high-resolution 2D maps produced from the seismic reflectivity could help improving the estimates of the parameters to be incorporated in numerical models of ocean dynamics.

ACKNOWLEDGEMENTS

This work has been fulfilled in the framework of the projects POSEIDON (Ref: CTM2010-25169) and APOGEO (Ref: CTM2011-16001-E/MAR), both funded by the Spanish Ministry of Economy and competitiveness (MINECO). The seismic and oceanographic data were acquired in the framework of the IMPULS survey (Ref: 2003-05996-MAR) also from MINECO, and SAGAS survey (Ref: CTM2005-08071-C03-02/MAR-SAGAS). Helpful comments were provided by Josep Lluis Pelegrí, the Barcelona Center for Subsurface Images (B-CSI), and Diana Francis and David M. Holland from the Center for Global Sea Level Change (CSLC) – NYUAD, Abu Dhabi UAE.

APPENDIX A

Table A1. Parameters used in text

Variable	Value	Description
f	0.00008613 s^{-1}	Coriolis f. at 36°
N	5 cph = 0.00138 s^{-1}	Buoyancy frequency (ocean average)
V	0.207 m s^{-1}	RMS amplitude of velocity fluctuations
υ	0.000001064 m^2 s^{-1}	Kinematic Viscosity
$\mathbf{C_T}$	0.4	Proportionality constant
$\boldsymbol{\Gamma}$	0.2	Empirical value of mixing efficiency (Osborn and Cox, 1972).

APENDIX B

Buoyancy Reynolds number

Gargett et al, (1988) use an index to know if the system is isotropic or not, and hence if the allowing know if the buoyancy flux is substantial to generate turbulence and therefore a high mixing level (Thorpe, 2005). The index depends on kinematic viscosity and is called Buoyancy Reynolds number:

$$R_B = \varepsilon / \nu N^2 \quad \text{(B1)}$$

The mean kinematic viscosity in the ocean is $\nu = 1 \times 10^{-6}\ m^2\ s^{-1}$. Some properties of the inertial subrange are consistent with isotropy for values of $R_B < O(10^2)$. To consider anisotropy and avoid serious underestimates of mixing, Smyth and Moum (2000) propose that values > 200 are related with confidence to high mixing levels due to free viscous effects. For our submesoscale regime $R_B = 3200$, a value that reasserts the coherence of the mixing levels calculated. The MCS data present a high confidence level.

References

Biescas B., B. R. Ruddick, M. R. Nedimovic, V. Sallarès, G Bornstein, and J. F. Mojica, Recovery of temperature, salinity, and potential density from ocean reflectivity, J. Geophys. Res. Oceans, 119, 3171-3184, doi:10.1002/2013JC009662, 2014.

Batchelor G. K., Small-scale variation of convected quantities like temperature in turbulent fluid, Fluid Mech., 5, 113-133, 1959.

Chioua J., Bruno M., Vazquez A., Reyes M., Gomiz J., Mañanes R., Alvarez O., Gonzalez C., Lopez L., Gomez-Enri J., Internal waves in the strait of Gibraltar and their role in the vertical mixing processes within the bay of Algeciras, Estuarine, Costal and Shelf Science, Elsevier, 126, 70-86, 2013.

D`Asaro Eric A., Lien Ren-Chien, The Wave-turbulence transition for stratified flows, Journal of physical Oceanography, 1669-1678, July, 2000.

Ferrari Raffaelle and Wunsch Carl, Ocean circulation kinetic energy: Reservoirs, sources, and sinks, Annu. Rev. Fluid Mech, 41: 253-282, 2009.

Fortin et. al., Mapping turbulent diffusivity associated with oceanic internal lee waves offshore Costa Rica. Ocean Sci., 12, 601-612, 2016.

Gargett A and Holloway G, Dissipation and diffusion by internal wave breaking, J. Mar. Res., 42, 15-27, 1984.

Gargett A., The scaling of turbulence in the presence of stable stratification, J. of Geophys. Res., 93, 5021-5036, 1988.

Garrett Christopher and Munk Walter, Internal waves in the ocean, Ann. Rev. Fluid Mech., 11, 339-369, 1979.

Gibson Carl., Keeler R., Bondur Valery, Leung Pak, Prandke H., Vithanage D., Submerged turbulence detection with optical satellites, Coastal Ocean Remote Sensing Conf., Paper 6680-33, San Diego, CA, 2007.

Gregg M. C., Diapycnal mixing in the thermocline: A review, Journal of geophysical research, Vol. 92, Number C5, 5249-5286, 1987.

Gregg M. C., Scaling turbulent dissipation in the thermocline, Journal of geophysical research, Vol. 94, Number C7, 9686-9698, 1989.

Haibin Song, Luis M. Pinheiro, Barry Ruddick and Xinghui Huang. Seismic Oceanography: A new geophysical tool to investigate the thermohalinestructure of the oceans, Oceanography, Prof. Marco Marcelli (Ed.), ISBN: 978-953-51-0301-1, InTech, 2012.

Henyey Frank S. and Wright Jon, Energy and action flow through the internal wave field: an Eikonal Approach, Journal of Geophysical Research, Vol. 91, No: C7, Pages 8487-8495, July 15, 1986.

Holbrook, W., Fer, I., Ocean internal wave spectra inferred from seismic reflection transects. Geophysical Research Letters, Vol. 32, L15604, doi:10.1029/2005GL023733. 2005.

Holbrook, W., Fer, I., Schmitt, R., Lizarralde, D., Klymak. J., Helfrich, C. and Kubichek, R., Estimating oceanic turbulence dissipation from seismic images, Journal of Atmospheric and Oceanic Technology, 2013.Ann. Rev. Fluid Mech., 40, 169-184, 2008.

Holbrook Steven, Fer Ilker, Schmitt Raymond, Lizarralde Daniel, Klymak Jody, Helfrich Cody, and Kubichek Robert, Estimating oceanic turbulence dissipation from seismic images, J. of Atmospheric and Oceanic Tech., Vol. 30, 1767-1788, doi:10.1175/JTECH-D-12-00140.1, 2013.

Klymak M. Jody, Moum N. James, Oceanic isopycnal slope spectra. Part a: Internal waves, Journal of Physical Oceanography. American Meteorological Society, Vol. 37, 1215-1231, 2007.

Klymak M. Jody, Moum N. James, Oceanic isopycnal slope spectra. Part b: Turbulence, Journal of Physical Oceanography. American Meteorological Society, Vol. 37, 1232-1244, 2007.

Kolmogorov, A., Dissipation of energy in the locally isotropic turbulence (English translation 1991). Proc. Roy. Soc. London, A434, 15–17. 1941.

Kunze, E., and Thomas B. Sandford. Abyssal Mixing: Where it is not. J. Phys. Oceanogr. 26, 2286-2296, 1996.

Laurent and Garrett, The role of internal tides in mixing the deep ocean. J. Phys. Oceanogr. 32, 2882-2899, 2002

Li Hua, Yamazaki Hidekatsu, Observations of Kelvin-Helmholz billow in the ocean, Journal of Oceanography, Vol. 57, 709-721, 2001.

Munk W. H., A survey of internal waves and small-scale processes, Evolution of Physical Oceanography, edited by B. A. Warren and C. Wunsch, pp. 264-291, MIT Press, Cambridge, Mass, 1981.

Munk W. Wunsch C., Abyssal recipes II: energetics of tidal and wind mixing, Deep-Sea Research I, Vol. 45, 1977-2010, 1998.

Müller, P. and R. Pujalet : Internal gravity waves and small scale turbulence, proceeding, 'Aha Huliko'a Hawaiian winter workshop, Hawaiian institute of geophysics, Special Publications, 299 pp., 1984.

Osborn T., & C. S. Cox, Oceanic fine structure, Geophys. Fluid Dyn., Vol. 3, 321-345, 1972.

Osborn T. R, Estimates of the local rate of vertical diffusion from dissipation measurements, Journal of Physical Oceanography, Vol. 10, 83-89, 1980.

Riley J. James, Stratified turbulence: A possible interpretation of some geophysical turbulence measurements, Journal of the Atmospheric Sciences. Vol. 65, 2416-2424, 2008.

Sallarès, V., J. F. Mojica, B. Biescas, D. Klaeschen, and E. Gracia, Characterization of the submesoscale energy cascade in the Alboran Sea thermocline from spectral analysis of high-resolution MCS data, Geophys. Res. Lett., 43, 6461-6468, doi:10.1002/2016GL069782.

Samodurov, A., S., Lubitsky, A., A., and Panteleev, N., A., Contribution of breaking internal waves to structure formation, energy dissipation, and vertical diffusion in the ocean. Phys. Oceanogr., Vol. 6, 3, pp 177 - -190, 1995.

Send Uwe, Font Jordi, Krahmann Gerd, Millot Claude, Rhein Monica, Tintore Joaquin, Recent advances in observing the physical oceanography of the western Mediterranean Sea. Elsevier Science. Progress in Oceanography. Vol. 44, 37-64, 1999.

Sheen L. K., White J. N., Hobbs R. W., Estimating mixing rates seismic images of oceanic structure, Geophysical Research Letters, Vol. 36, L00D04, 2009.

Sheriff Robert and Geldart Lloyd, Exploration Seismology, Cambridge University Press, Second edition, 1995.

Smyth W. D., Moum J. N., Nash J. D., Narrowband oscillations in the upper equatorial ocean. Part II:Properties of shear instabilities, Journal of Physical Oceanography. American Meteorological Society, Vol. 41, 412-428, 2011.

Sreenivasan Katepalli, The passive scalar spectrum and the Obukhov-Corrsin constant, Phys. Fluids, 8, 189-196, 1996.

Smyth William D., Moum James N., Anisotropy of turbulence in stably stratified mixing layers, Physics of Fluids, 12, No. 6, 2000.

Smyth William D., Moum James N., Ocean mixing by Kelvin-Helmholtz Instability, Oceanography, Vol. 25, No. 2, June 2012.

Stewart Robert, Introduction to Physical Oceanography, Department of Oceanography, Texas A&M University, 2008.

Taylor G. I., The spectrum of turbulence, Proc. R. Soc. Lond. A., Vol. 164, No. 919, 476-490, 1937.

Thorpe S. A., Experiments on the instability of stratified shear flows: miscible fluids, J. Fluid Mech., Vol. 46, 299-319, 1971.

Thorpe S. A., The turbulent ocean, Cambridge University Press, Cambridge, 2005.

Waite, Michael L., Stratified turbulence at the buoyancy scale, Physics of fluids, American Institute of Physics, 23, 066602-1, June 2011.

Wesson J.C. and Gregg M.C., Mixing at camarinal sill in the strait of Gibraltar, Journal of Geophysical Research, Vol. 99, No. C5, pages 9847-9878, May 15, 1994.

Woods, J., D.,: Wave induced shear instability in the summer thermocline, J. Fluid Mech., 32, 791-800., 1968.

Wunsch Carl and Ferrari Raffaele, Vertical Mixing, energy, and the general circulation of the oceans, Annual Review Fluid Mech. 36, p. 281-314, 2004.

Yilmaz, O., and S. M. Doherty, Seismic Data Processing, Soc. Of Explor. Geophys, Tulsa, Okla 1987

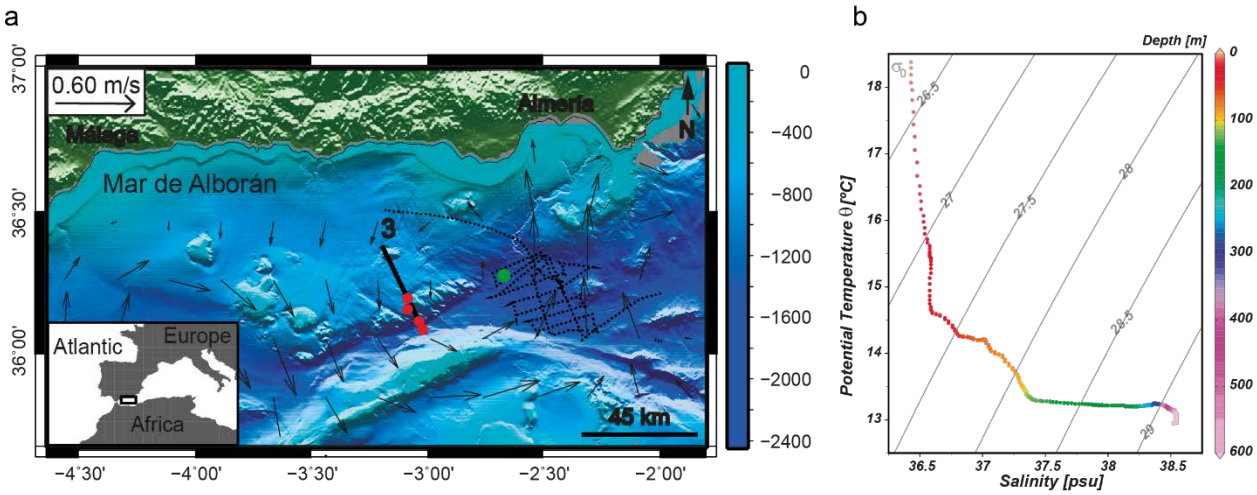

Figure 1. (a) Bathymetric map of the Alboran Sea and location of the data used in the study. HR-MCS profile acquired during the IMPULS-2006 experiment (black line labelled 3), eXpendable Bathy-Thermograph (XBTs) profilers (red circles), eXpendable Conductivity Temperature Depth (XCTD) probe (green circle). Acoustic Doppler Current Profiler (ADCP) lines (black dotted line). Geostrophic velocity for May 17th, 2006 (gray arrows). (b) Temperature-Salinity diagram from XCTD probe. σ_0 is the potential density in kg/m^3. Color scale indicates depth.

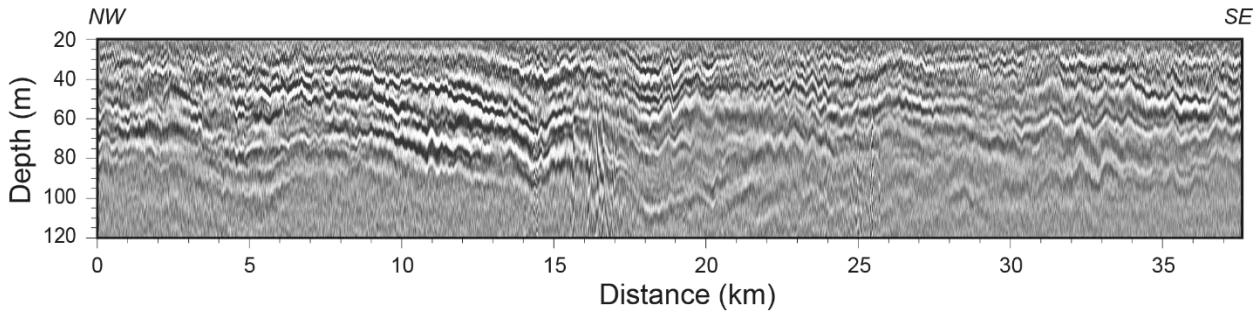

Figure 2. Depth-converted high-resolution multichannel seismic profile (See Fig. 1a for location).

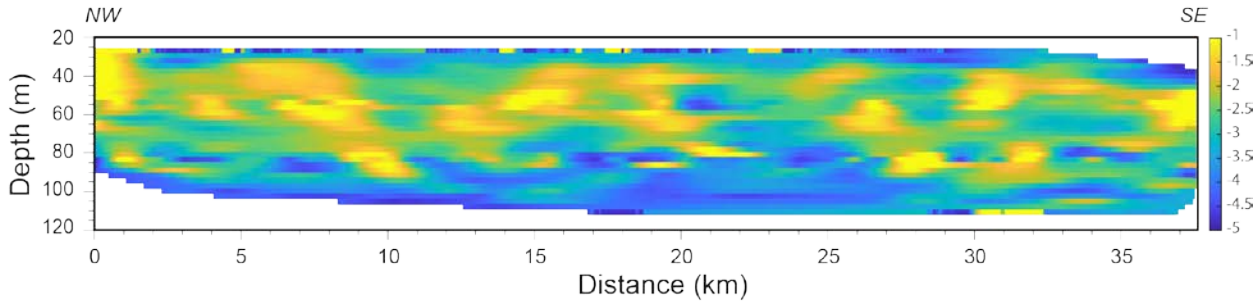

Figure 3. $k_\rho(x, z)$ map obtained along the seismic profile indicated in Fig.1, following the procedure explained in the text.

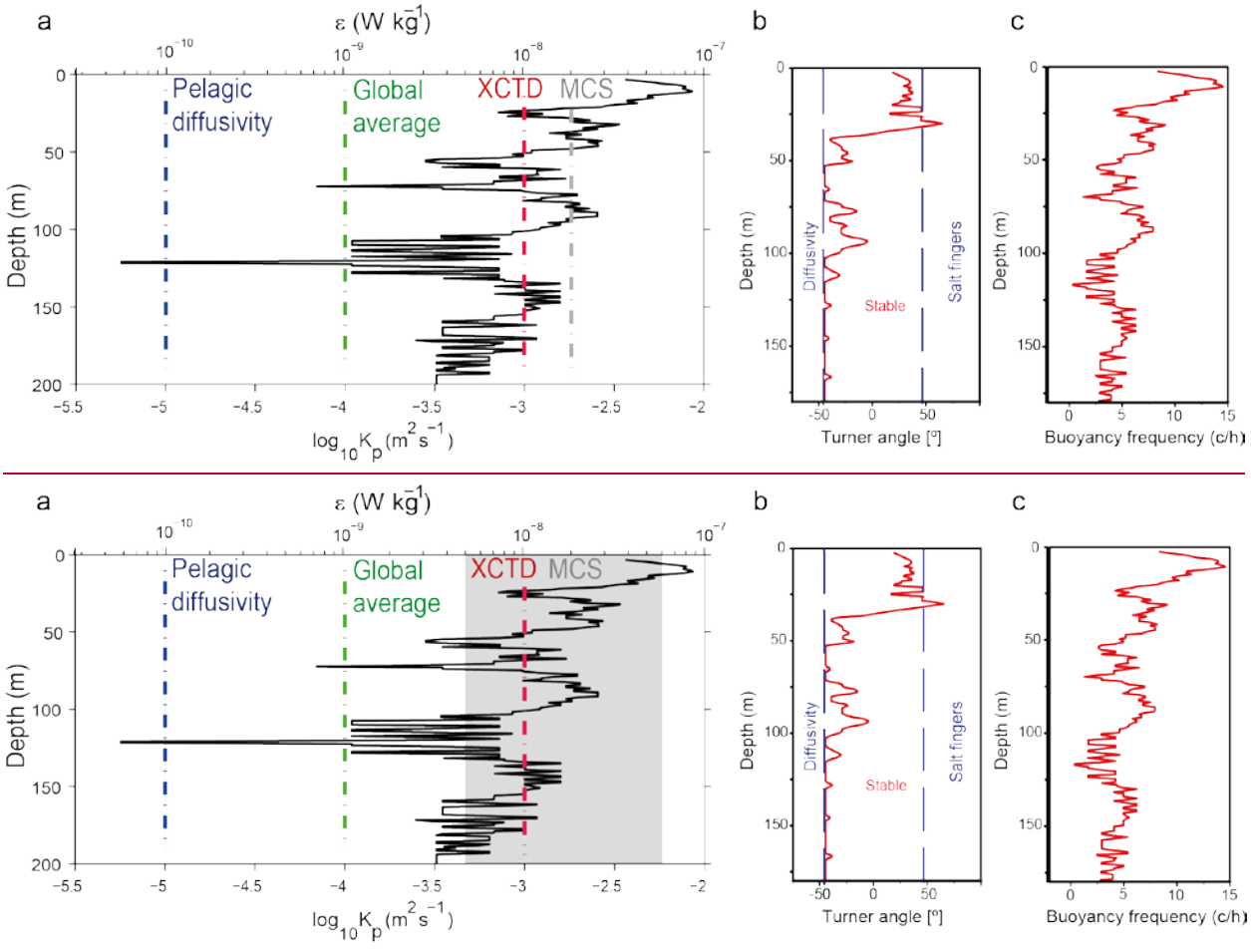

Figure 4. (a) Depth profile of $\varepsilon(z)$ and $k_\rho(z)$ obtained from XCTD and ADCP data and applying Gregg89 model. The blue dotted line is the pelagic diffusivity in the ocean ($k_\rho \approx 10^{-5}\ m^2s^{-1}$), the green dotted line is the global average for overturning ($k_\rho \approx 10^{-4}\ m^2s^{-1}$), the red dotted line is the average vertical profile from XCTD and ADCP data ($k_\rho \approx 10^{-3.0}\ m^2s^{-1}$) and the gray area~~dotted line~~ is the incidence range~~average vertical profile~~ from MCS data ($k_\rho \approx 10^{-2.7}\ m^2s^{-1}$). (b) Turner angle showing ranges, the blue dotted lines shows where the water column is unstable to diffusivity ($Tu<-45°$), stability ($-45° < Tu <45°$) and prone to salt fingering ($Tu > 45°$), and (c) buoyancy profile calculated with the XCTD data.

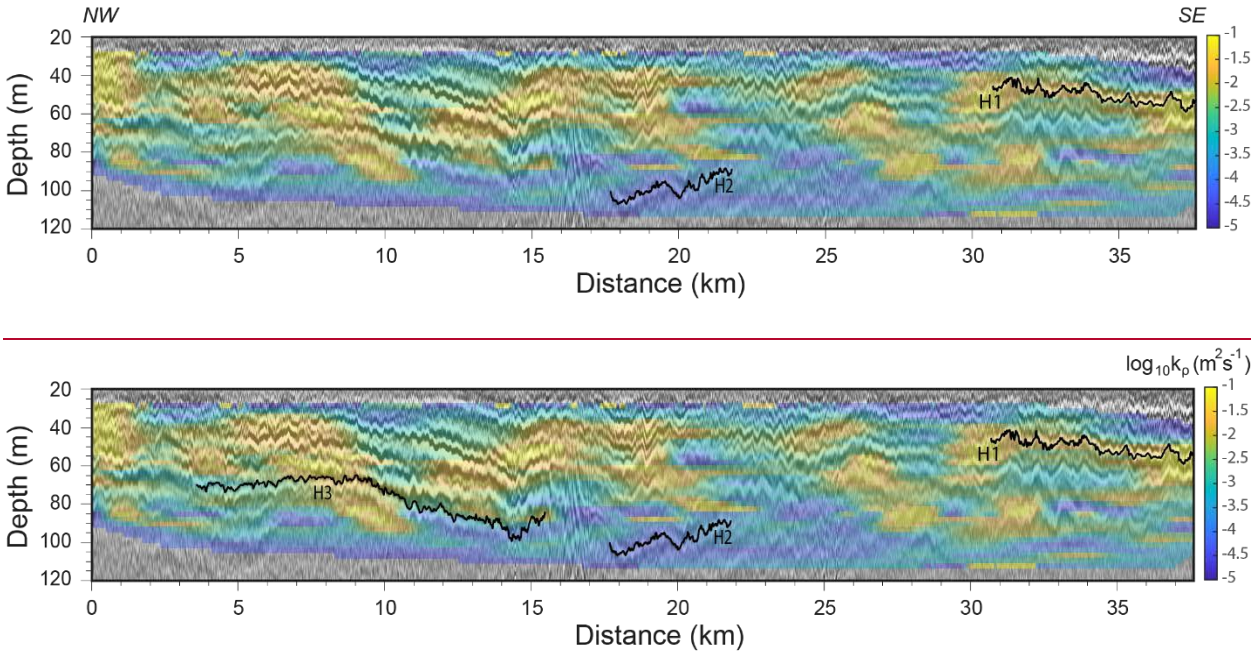

Figure 5. High-resolution $k_\rho(x, z)$ map overlapped with the HR-MCS image. Solid lines labelled H1, ~~and~~ H2 and H3, display acoustic reflectors located within relatively high- and low-dissipation areas from Batchelor model.

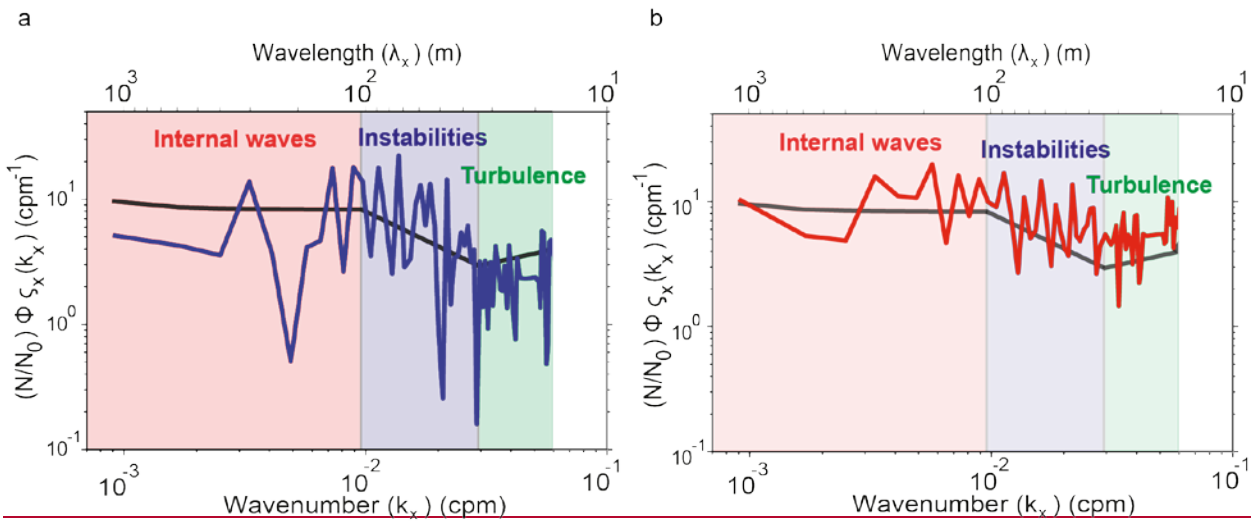

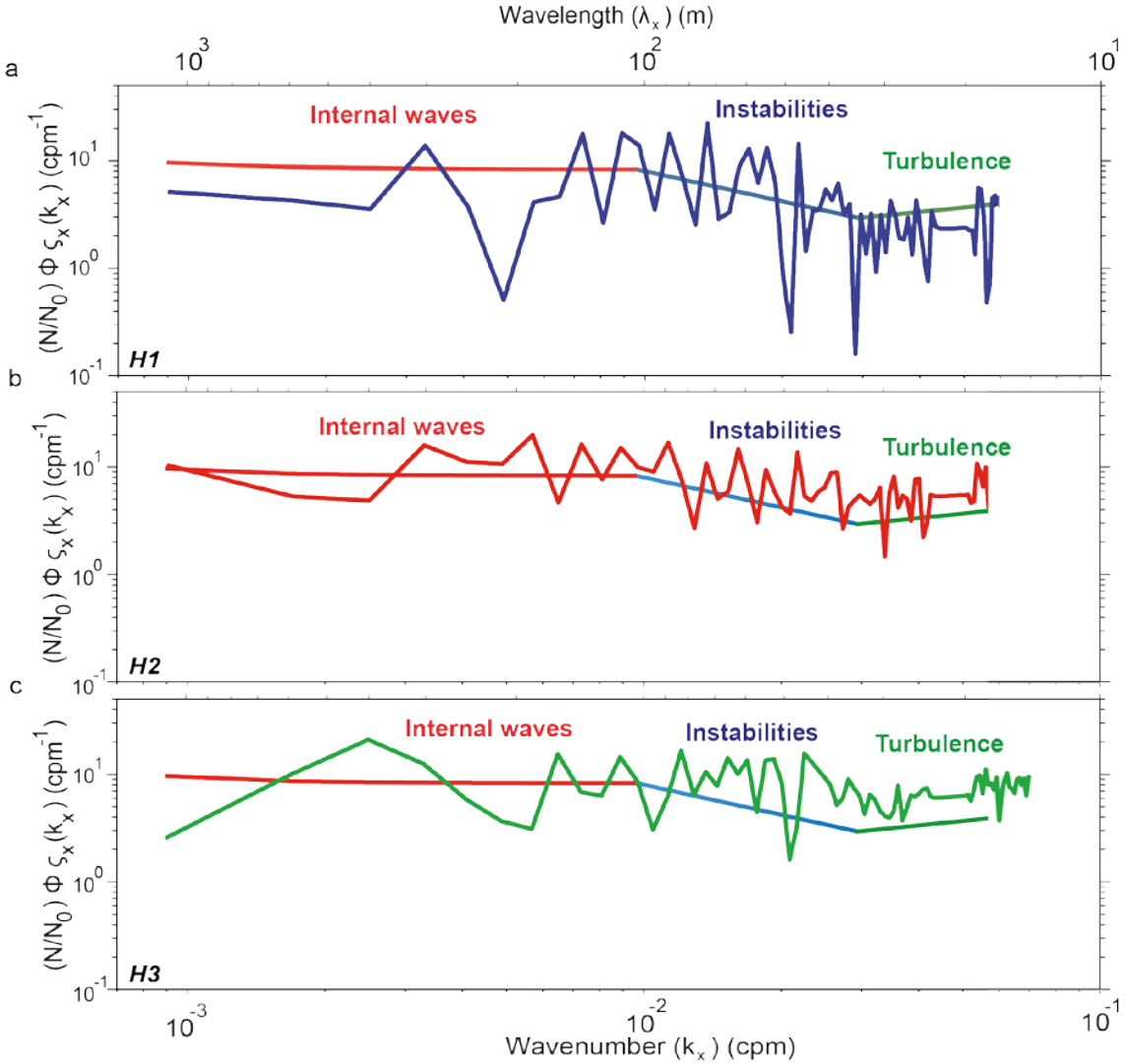

Figure 6. (a) Horizontal spectrum of the vertical displacement of reflector H1 (thick blue line) (see location in Fig. 5). ~~(Black line)~~ Reference line that follows theoretical slopes of Garret-Munk internal wave model (Garret and Munk, 1979) (red line), Kelvin-Helmholtz instabilities (Waite,

2011) (blue line), and Batchelor model for turbulence (Batchelor, 1959) (green line). The methodology applied to calculate the spectra is described in Sallares et al (2016), (b) and (c) same as in (a) for reflector H2 (red) and H3 (green) in this case.

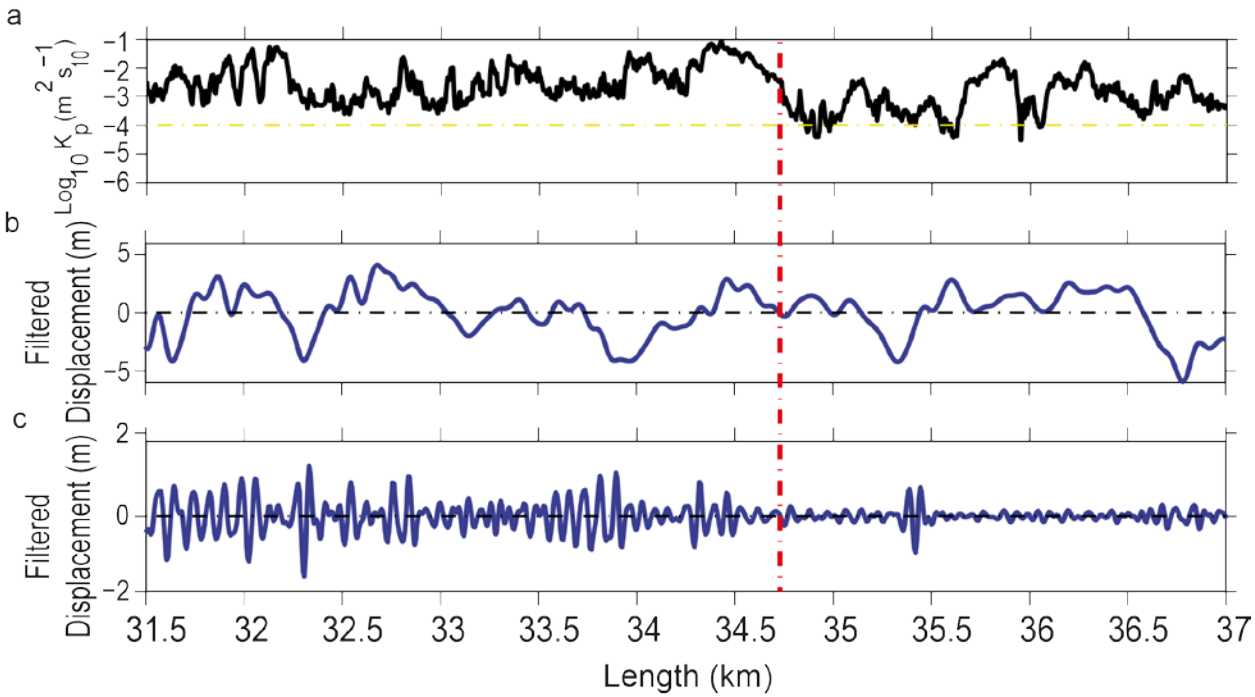

Figure 7. (a) Diapycnal mixing obtained along H1 (see details of calculation in the text). (b) Signal filtered at wavelength ranges of the IW sub-range (*3000-100 m*), (c) and the transitional subrange (*100-33 m*). The dashed red line identifies the "breaking point" referred to in the text.

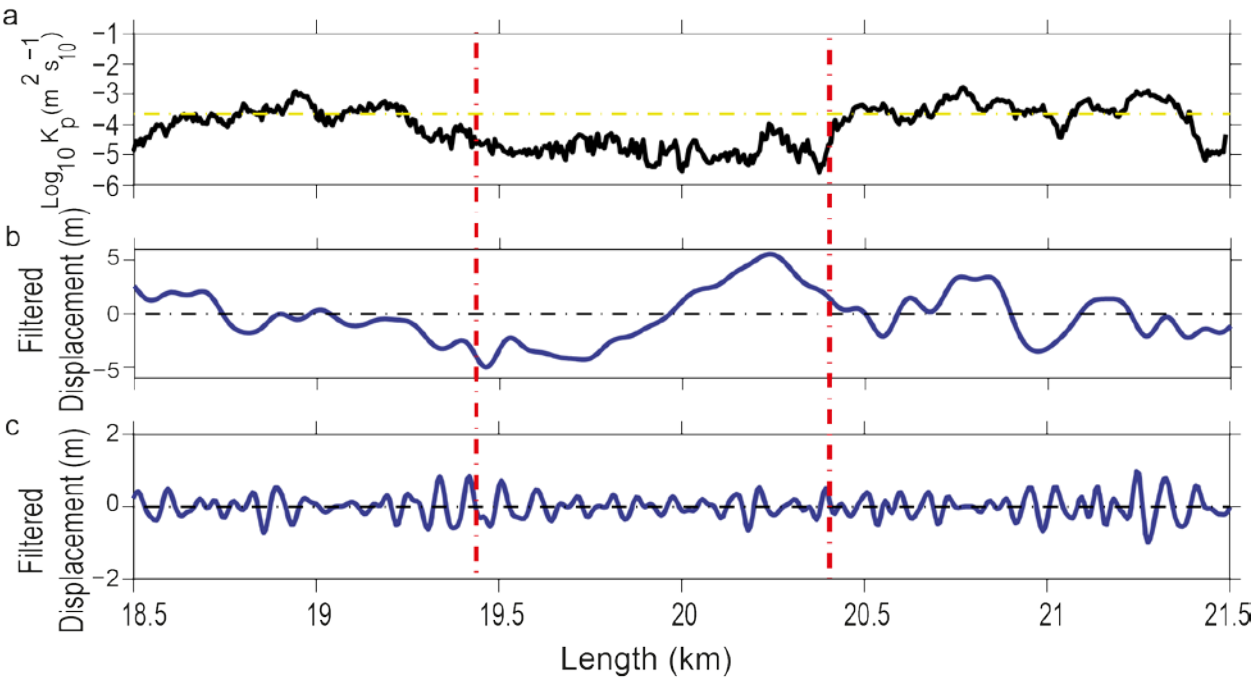

Figure 8. (a) Diapycnal mixing obtained along H2 (see details of calculation in the text). (b) Signal filtered at wavelength ranges of the IW sub-range (*3000-100 m*), (c) and the transitional subrange (*100-33 m*). The dashed red lines identifies the "breaking segment" referred to in the text.

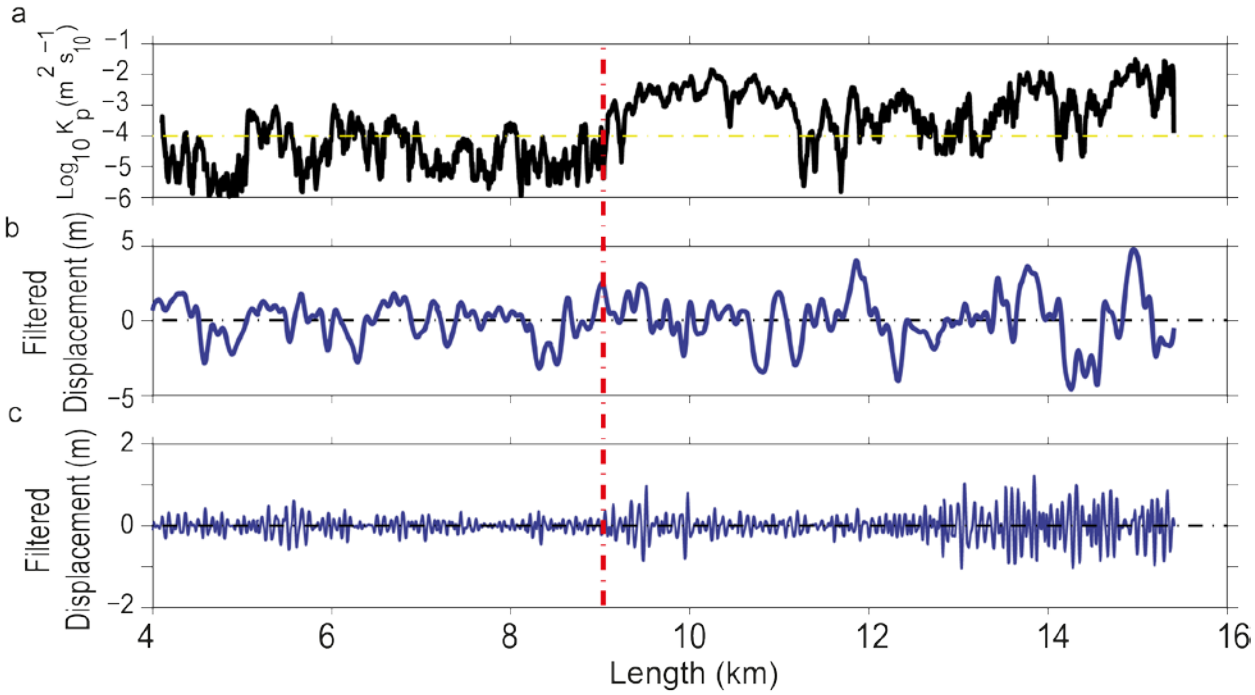

Figure 9. (a) Diapycnal mixing obtained along H3 (see details of calculation in the text). (b) Signal filtered at wavelength ranges of the IW sub-range (*3000-100 m*), (c) and the transitional subrange (*100-30 m*). The dashed red line identify the "breaking segment" referred to in the text.

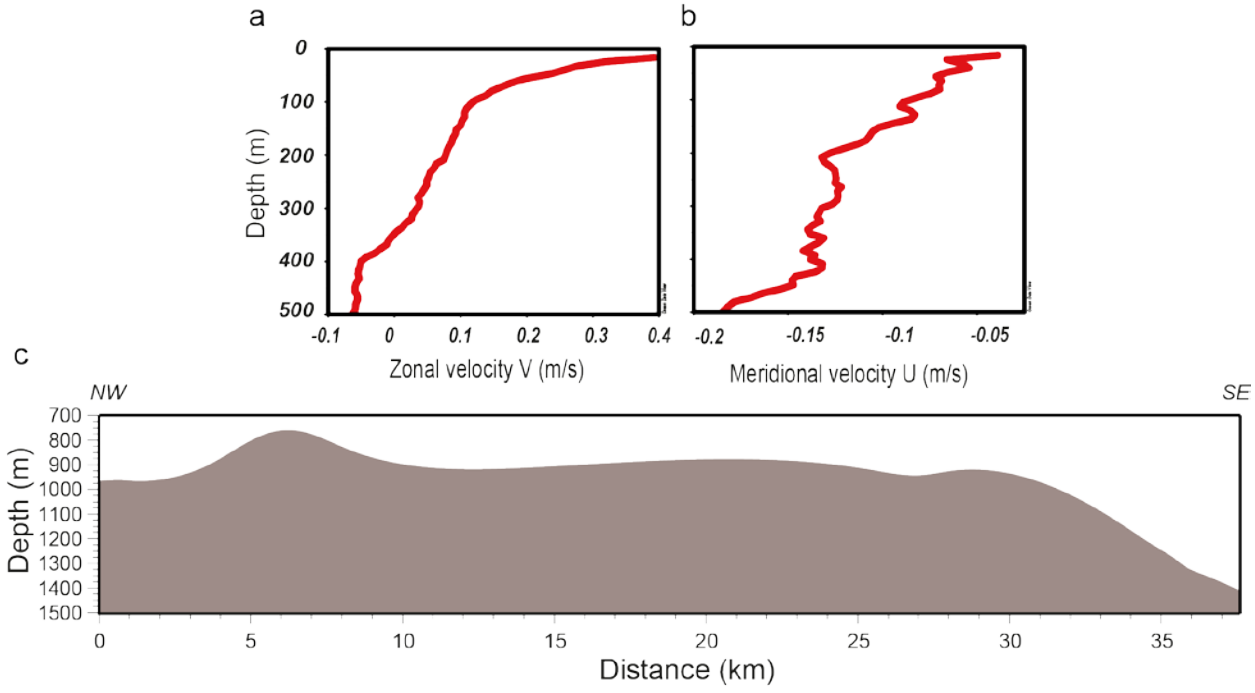

Figure ~~9~~10. (a) Current velocity profile from ADCP data, SAGAS in May, 2010. (*V*) The zonal velocity variations, and (b) (*U*) the meridional velocity variations according to the depth. (c) Bathymetric profile over the seismic profile.